Department of Applied Physics

Escape Rates of Externally Confined Polymers

Harri Mökkönen

Aalto University

DOCTORAL DISSERTATIONS

Aalto University publication series
DOCTORAL DISSERTATIONS 143/2016

Escape Rates of Externally Confined Polymers

Harri Mökkönen

A doctoral dissertation completed for the degree of Doctor of Science (Technology) to be defended, with the permission of the Aalto University School of Science, at a public examination held at the lecture hall M1 of the school on 19 August 2016 at 12.

This doctoral thesis is conducted under a convention for the joint supervision of thesis at Aalto University (Finland) and University of Iceland (Iceland)

Aalto University
School of Science
Department of Applied Physics
Multiscale Statistical Physics

Supervising professor
Tapio Ala-Nissilä, Aalto University, Finland

Thesis advisor
Hannes Jónsson, University of Iceland, Iceland

Preliminary examiners
Dmitrii E. Makarov, The University of Texas at Austin, U.S.A.
Wokyung Sung, Pohang University of Science and Technology, Republic of Korea

Opponent
Graeme Henkelman, The University of Texas at Austin, U.S.A.

Aalto University publication series
DOCTORAL DISSERTATIONS 143/2016

ISBN 978-952-60-6925-8 (printed)
ISBN 978-952-60-6924-1 (pdf)
ISSN-L 1799-4934
ISSN 1799-4934 (printed)
ISSN 1799-4942 (pdf)
http://urn.fi/URN:ISBN:978-952-60-6924-1

Unigrafia Oy
Helsinki 2016

Finland

441 697
Printed matter

Aalto University

Abstract

Aalto University, P.O. Box 11000, FI-00076 Aalto www.aalto.fi

Author
Harri Mökkönen

Name of the doctoral dissertation
Escape Rates of Externally Confined Polymers:

Publisher School of Science

Unit Department of Applied Physics

Series Aalto University publication series DOCTORAL DISSERTATIONS 143/2016

Field of research Theoretical and computational physics

Manuscript submitted 17 May 2016 **Date of the defence** 19 August 2016

Permission to publish granted (date) 28 June 2016 **Language** English

☐ **Monograph** ☒ **Article dissertation** ☐ **Essay dissertation**

Abstract

A polymer escaping from a confining external potential represents a generic description of long macromolecules crossing an energy barrier. This type of barrier crossing problems are typical in nano- and microscale polymeric systems, where the polymers are escaping from entropic traps by thermal fluctuations. These systems have possible bioengineering applications, where they can be for example used in sorting polymers. In this thesis, polymer escape from one- and two-dimensional external potentials was studied theoretically and computationally.

In a two-dimensional asymmetric external potential, the escape rate of a polymer was solved using Path Integral Hyperdynamics (PIHD) simulations and Kramers' theory using effective potentials for different lengths of polymers. We found that Kramers' theory predicts the escape rate of PIHD simulations qualitatively but the prediction agrees quantitatively only for shorter chains. We also determined that a one-dimensional reaction coordinate is not sufficient to describe the dynamics of the longer polymer chains.

In a one-dimensional symmetric double-well external potential, the escape rate was solved using Langevin dynamics simulations, Brownian dynamics simulations, harmonic transition state theory (HTST) with dynamical corrections (DC), Langer's theory, and Forward flux sampling (FFS). FFS and HTST with DC both predict the rate by Langevin and Brownian dynamics simulations quantitatively within a factor of two. We also introduced a new method for computing dynamical corrections using forward flux sampling type of algorithm and compared computational efficiency of the different methods.

Keywords polymers, molecular dynamics,transition state theory

ISBN (printed) 978-952-60-6925-8 **ISBN (pdf)** 978-952-60-6924-1

ISSN-L 1799-4934 **ISSN (printed)** 1799-4934 **ISSN (pdf)** 1799-4942

Location of publisher Helsinki **Location of printing** Helsinki **Year** 2016

Pages 103 **urn** http://urn.fi/URN:ISBN:978-952-60-6924-1

A! Aalto-yliopisto

Tiivistelmä

Aalto-yliopisto, PL 11000, 00076 Aalto www.aalto.fi

Tekijä
Harri Mökkönen

Väitöskirjan nimi
Polymeerien pakonopeus rajoittavasta ulkoisesta potentiaalista

Julkaisija Perustieteiden korkeakoulu

Yksikkö Teknillisen fysiikan laitos

Sarja Aalto University publication series DOCTORAL DISSERTATIONS 143/2016

Tutkimusala Teoreettinen ja laskennallinen fysiikka

Väitöspäivä 19.08.2016

☐ **Monografia** ☒ **Artikkeliväitöskirja** ☐ **Esseeväitöskirja**

Tiivistelmä

Polymeerin pako-ongelma ulkoisesta rajoittavasta potentiaalista on yleinen kuvaus makromolekyylien energiavallin ylityksestä. Tämän tyyppiset energiavallin ylitykset ovat tyypillisiä mikro- ja nanoskaalan polymeerisysteemeistä, joissa polymeeri pakenee termisten fluktuaatioden ansiosta entroppisesta energiakuopasta. Tällaisilla systeemeillä on sovelluskohteita bioinsinööritieteissä, esimerkiksi polymeerien lajittelussa niiden pituuden perusteella. Tässä väitöskirjassa on numeerisesti tutkittu polymeerien pako-ongelmaa yksi- ja kaksiulotteisessa systeemissä.

Kaksiulotteisessa epäsymmetrisessa ulkoisessa potentiaalissa pakonopeus on selvitetty polkuintegraalihyperdynamiikkasimulaatioilla ja Kramersin teorialla käyttäen efektiivisiä potentiaaleja eri mittaisille polymeereille. Kramersin teoria ennustaa pakonopeuden kvalitatiivisesti oikein, mutta ennuste on kvantitatiivisesti tarkka vain lyhyille polymeeriketjuille. Työssä on myös todettu, että yksidimensioinen reaktiokoordinaatti ei ole riittävän tarkka kuvaamaan pakoprosessia pidemmille ketjuille.

Yksiulotteisessa, symmetrisessä ja kaksoiskaivon muotoisessa ulkoisessa potentiaalissa pakonopeus laskettiin käyttämällä Langevinin ja Brownin dynamiikka-simulaatioita, sekä harmonista transitiotilateoriaa dynaamisilla korjauksilla, Langerin teoriaa ja "forward flux sampling"-menetelmää. "Forward flux sampling"-menetelmä sekä harmoninen transitiotilateoria dynaamisilla korjauksilla ennustavat kvantitatiivisen tarkasti Langevinin ja Brownin dynamiikalla lasketun pakonopeuden. Dynaamisille korjauksille esitettiin myös uudentyyppiinen "forward flux sampling" menetelmään perustuva algoritmi sekä verrattiin eri menetelmien laskennallista tehokkuutta.

Avainsanat polymeeri, molekyylidynamiikka, transitiotilateoria

ISBN (painettu) 978-952-60-6925-8	**ISBN (pdf)** 978-952-60-6924-1	
ISSN-L 1799-4934	**ISSN (painettu)** 1799-4934	**ISSN (pdf)** 1799-4942
Julkaisupaikka Helsinki	**Painopaikka** Helsinki	**Vuosi** 2016
Sivumäärä	**urn** http://urn.fi/URN:ISBN:978-952-60-6924-1	

Aalto University

Abstract

Aalto University, P.O. Box 11000, FI-00076 Aalto www.aalto.fi

Author
Harri Mökkönen

Name of the doctoral dissertation
Sleppihraði aðþrengdra fjölliða

Publisher School of Science

Unit Department of Applied Physics

Series Aalto University publication series DOCTORAL DISSERTATIONS

Field of research Theoretical and computational physics

Manuscript submitted 16 May 2016 **Date of the defence** 19 August 2016

Permission to publish granted (date) 28 June 2016 **Language** English

☐ **Monograph** ☒ **Article dissertation** ☐ **Essay dissertation**

Abstract
Í líftækni er áhugi á kerfum þar sem stórum sameindum er haldið á takmörkuðu svæði með ytra mætti þar til þær sleppa út við það að yfirstíga fríorkuhól fyrir tilstilli varmafræðilegrar örvunar. Dæmi um slík kerfi eru nanó eða míkróskala entrópíugildrur sem notaðar eru til að aðgreina fjölliður. Í þessari ritgerð er lýst kennilegum rannsóknum og reikningum á sleppihraða fjölliða í tví- og þrívíðum kerfum.

Sleppihraði fjölliða af ýmsum lengdum var reiknaður fyrir ósamhverft mættisfall með því að nota feriltegur háhreyfijöfnu (PIHD) og aðferð Kramers. Niðurstöður reikninganna voru í mjög góðu samræmi við beina reikninga fyrir stuttar fjölliður en ekki nema í grófu samræmi fyrir langar fjölliður. Þetta sýnir að einvíð hvarfstika nægir ekki til að lýsa færslu langra fjölliða.

Sleppihraðinn fyrir samhverft mættisfall með tveimur orkubrunnum var reiknaður með ýmsum aðferðum, svo sem Langevin hreyfijöfnu, Brown hreyfijöfnu, virkjunarástandskenningu innan kjörsveifilsnálgunar (HTST) með leiðréttingu frá tímaferlum (DC) og áframflæði reikningum (FFS). FFS og HTST/DC aðferðirnar gefa báðar mat á sleppihraðanum í góðu samræmi við Langevin og Brown hreyfijöfnur. Ný aðferð til að reikna DC sem nýtir eiginleika FFS var sett fram og reikniþörfin borin saman við aðrar aðferðir.

Keywords fjölliður, klassískir ferlar, virkjunarástandskenningin

ISBN (printed) 978-952-60-6925-8 **ISBN (pdf)** 978-952-60-6924-1

ISSN-L 1799-4934 **ISSN (printed)** 1799-4934 **ISSN (pdf)** 1799-4942

Location of publisher Helsinki **Location of printing** Espoo **Year** 2016

Pages 103 **urn** http://urn.fi/URN:ISBN:978-952-60-6924-1

Preface

The work presented in this thesis was carried out during 2013-2016 in the Multiscale Statistical Physics group (MSP) in the Department of Applied Physics at the Aalto University School of Science. Most of the work has been done in close collaboration with the Faculty of Physical Sciences at the University of Iceland.

This work has been supported by the FiDiPro programme of the Academy of Finland and travel during this work by the Education Network in Condensed Matter and Materials Physics. Computational resources have been provided by Aalto Science-IT project and CSC - IT Center for Science. The MSP group is part of the Centre of Excellence in Computational Nanoscience (COMP) funded by the Academy of Finland.

I would like thank my supervisor Prof. Tapio Ala-Nissilä from Aalto University for providing me this opportunity to do this doctoral thesis. I started working with Tapio as a summer student in 2011 and he also supervised my master's thesis. Under Tapio's supervision, I have learned a lot, ranging from the English grammar to the fundamentals of statistical physics and the nature of the academic world. Also, special thanks go to Prof. Hannes Jónsson from the University of Iceland who has instructed and helped me along this thesis and provided very valuable insights on the problems that I have been studying. Big thanks for both professors for giving me a lot of opportunities to visit the University of Iceland and Iceland in general. I am grateful for the many possibilities to participate in international conferences and summer schools. Also thanks to previous MSP member Dr. Timo Ikonen for simulation codes, encouraging discussions and input on the articles.

I wish to thank all my colleagues in the MSP group. Thanks also to Dr. Aki Kutvonen and M. Sc. Samu Suomela for the travel company and my office mates Dr. Vaibhav Thakore and M. Sc. Michiko Alcanzare, to

mention, for the answers to my questions. Special thanks to Dr. Vili Heinonen and Dr. Tuukka Hiltunen for the casual, nearly everyday tea breaks and lunch company. Also thanks to my other friends for the lunch company and other fun activities during the years, Dr. Mikko Kataja, M. Sc. Patrik Laiho, Lic. Olli Heikkinen, M. Sc. Pauli Koski, to mention.

Doing my doctoral studies has not been always easy. I want to thank my family, especially my parents, for supporting and encouraging me during the darkest moments of this work.

"So long, and thanks for all the fish."

-Douglas Adams, The Hitchhiker's Guide to the Galaxy

Espoo, July 6, 2016,

Harri Mökkönen

Contents

List of Publications

This thesis consists of an overview and of the following publications which are referred to in the text by their Roman numerals.

I Harri Mökkönen, Timo Ikonen, Hannes Jónsson, Tapio Ala-Nissilä. Polymer escape from a confining potential. *Journal of Chemical Physics*, 140, 054907, February 2014.

II Harri Mökkönen, Timo Ikonen, Tapio Ala-Nissilä, Hannes Jónsson. Transition state theory approach to polymer escape from a one dimensional potential well. *Journal of Chemical Physics*, 142, 224906, June 2015.

III Harri Mökkönen, Tapio Ala-Nissilä, Hannes Jónsson. Efficient dynamical correction of the transition state theory rate estimate for a flat energy barrier. *Journal of Chemical Physics*, Submitted, May 2016.

Author's Contribution

Publication I: "Polymer escape from a confining potential"

The author carried out the computer simulations and wrote the manuscript with the co-authors.

Publication II: "Transition state theory approach to polymer escape from a one dimensional potential well"

The author carried out the computer simulations and wrote the manuscript with the co-authors.

Publication III: "Efficient dynamical correction of the transition state theory rate estimate for a flat energy barrier"

The author carried out the computer simulations and wrote the manuscript with the co-authors.

1. Introduction

The polymer escape problem is a generic description of a long macromolecule escaping from a confining external potential. In the problem, a polymer escapes from an initial metastable state by thermal activation by crossing an energy barrier. The barrier can be of entropic origin due to geometric confinement, in which case it becomes a free energy barrier, or of electromagnetic origin for polyelectrolytes, in which case it can be modelled by an external potential function. When there is no external potential barrier present, the barrier is purely entropic. In the polymer escape problem, there is an entropic barrier present in addition to the bare external potential.

Experimental examples of relevant systems include polymer translocation [1, 2], where a polymer crosses a membrane through a pore [3], or narrow μm-scale channels with traps [4]. Recent experiments by Liu *et al.* involve the escape of DNA molecules from an entropic cage [5]. Similar translocation and escape processes are common in cell biology and have possible bioengineering applications, such as DNA sequencing [6] and biopolymer filtration [7].

Polymer escape is often a rare event, which makes it difficult to model it with conventional numerical simulation methods. The problem exhibits a separation of time scales; the internal vibrational time scale of a polymer chain is orders of magnitude faster than the time scale of the actual escape. In molecular dynamics simulations, the fast vibrations in the polymer chain need to be explicitly modelled, which consumes most of the simulation time, and infrequent escape events are not efficiently sampled. Rate theories and accelerated simulation methods can be introduced to address this problem.

Kramers [8] has developed a theory for a one-dimensional particle escaping from an external potential well, which was later generalised to

multidimensional systems by Langer [9]. The first theory for a polymer escaping from an external potential well was developed by Park and Sung [10] who evaluated the escape rate of a discrete ideal polymer from an asymmetric potential well using lattice statistics.

Sebastian [11] has proposed a kink diffusion mechanism for long chains when one end of the polymer has moved over the barrier, while the other end is still in the initial state. The kink corresponds to the beads in the region of the energy barrier, and it moves along the chain as the polymer moves from one potential well to another. In Ref. 12, Sebastian and Paul describe the polymer escape of long chains as a two-step process. In the first step, the polymer is thermally activated to bring one end over the energy barrier and into the final state, and the second step involves diffusive motion of the kink as intermediate beads move in and out of the barrier region. A rate theory approach similar to Langer's [9] multidimensional extension of Kramers' theory was proposed for activation [12]. More recently, Sebastian and Debnath studied the thermal activation mechanism for short chains [13] and simulated kink diffusion for one- and three-dimensional systems [14].

Lee and Sung studied polymer escape in a symmetric external potential well and proposed a rate theory approach to predict the rate for linear [15] and for semiflexible ring polymers [16]. They also found that for linear polymers, the stretched kink solution is the dominant escape mechanism for chains longer than a certain crossover length N_C. Below N_C, the polymer crosses the barrier in a coiled form while polymers that are longer than N_C are stretched during the transition, analogous to instantons in quantum mechanical tunnelling of a particle. Paul [17] has studied the escape problem of star polymers in a system mimicking experiments carried out by Han *et al.* [4].

The polymer escape problem with an asymmetric external potential well has previously been studied numerically using path integral hyperdynamics by Shin *et al.* [18] and by Ikonen in his doctoral thesis [19].

In this thesis, we study numerically the polymer escape problem in one- and two-dimensional systems. We perform molecular dynamics (MD) simulations and then use rate theories to predict the escape rate obtained by MD. A confining two-dimensional external potential and a one-dimensional, bistable, double-well external potential are studied with various polymer chain models. We mainly focus on solving the escape rate but also examine the configurations that the polymer takes during the escape.

This thesis is organised as follows. In Sec. 2 we give a short review of the theoretical background presenting the used polymer models and potential functions. In the section the existing rate theories such as Kramers' theory, Langer's theory and the harmonic transition state theory (HTST) are introduced. Numerical methods including Langevin dynamics (LD) simulation, Path integral hyperdynamics (PIHD), Nudged elastic band (NEB) and Forward flux sampling (FFS) are presented in Sec. 3.

In Sec. 4 we present the results of this thesis. The results describe the effect of external confinement to the polymer escape dynamics in the two dimensional well. The results also show that instead of numerically heavy LD simulations, the quantitatively correct escape rate can be obtained with HTST followed by dynamical corrections (DC) and with FFS. We show that the HTST with DC obtains better estimate for the escape rate than previously used Langer's theory when compared with LD simulations. We present novel way of computing DC using FFS type of algorithm. In Sec. 5 we summarise and discuss the results.

2. Theory

2.1 Problem description

In the theoretical description of the polymer escape, a polymer is initially placed in a confining external potential well. The polymer is coupled to a heat bath and after long enough time it has reached thermal equilibrium in the initial state. At a long enough time scale, the polymer eventually escapes over the energy barrier by thermal activation. The polymer escape is a rare event since the time scale of the actual escape is orders of magnitude longer than the time scale of internal relaxation of the polymer chain. In Fig. 2.1 the polymer escape for a self-avoiding chain escaping from a two-dimensional asymmetric external potential is visualised.

The polymers here are modelled using the canonical bead-spring model [20, 21] where individual beads (monomers) are connected with springs. The system is described by the Hamiltonian

$$\mathcal{H}(\{\mathbf{r}_i, \mathbf{v}_i\}) = \sum_{i=1}^{N} \frac{m}{2}|\mathbf{v}_i|^2 + E(\{\mathbf{r}_i\}), \tag{2.1}$$

where the $\mathbf{r}_i$ and $\mathbf{v}_i$ are the positions and velocities of the beads, respectively, m is the mass of an individual bead, and E the total potential energy functional of the system. The total potential energy consist of an external potential energy and the interaction potential energy between the monomers as: $E(\{\mathbf{r}_i\}) = V(\mathbf{r}_i) + U(\{\mathbf{r}_i\})$, where $V(\mathbf{r}_i)$ is the external potential and $U(\{\mathbf{r}_i\})$ the interaction potential.

Real polymers are usually in a solvent, so a convenient choice for describing their dynamics is the Langevin equation which allows us to model the hydrodynamic interactions using simplest approximation where the solvent acts as a dissipative heat bath to the polymer. Thus, Langevin equation does not take hydrodynamics explicitly into account. To this end,

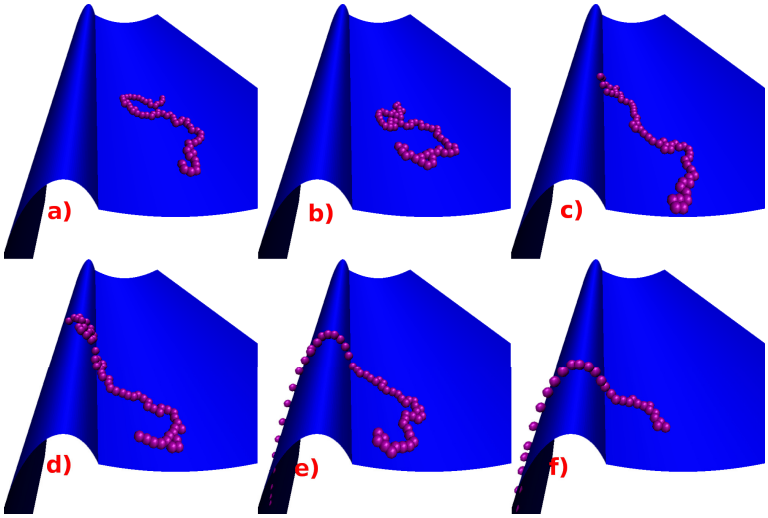

Figure 2.1. An example of a polymer escaping from a potential well visualised using data from molecular dynamics simulations. The blue surface represents the potential energy surface of the external potential well. a) The polymer is in its initial configuration after equilibration. b) The polymer exhibiting a coiled state. c) The polymer in a stretched state. d) The polymer starting to surmount the barrier. e) The polymer at the limit after which it is considered to have crossed the barrier. f) The polymer is almost completely over the barrier.

other coarse-grained simulation methods such as the fluctuating lattice-Boltzmann method [22] should be used. In Langevin dynamics, the equation for one particle is

$$m\ddot{\mathbf{r}}(t) + \gamma\dot{\mathbf{r}}(t) + \nabla E(\mathbf{r}) = \xi(t), \tag{2.2}$$

where γ is the friction coefficient. A Gaussian random force $\xi(t)$ describes the effect of collisions by the solvent molecules and is defined in such a way that $\langle\xi(t)\rangle = 0$ and $\langle\xi_\mu(t)\xi_\nu(t')\rangle = 2\gamma k_B T\delta_{\mu,\nu}\delta(t-t')$. Here $\langle\dots\rangle$ denotes the ensemble average, μ and ν Cartesian coordinate indices, k_B the Boltzmann constant, T the temperature, $\delta(t)$ the Dirac delta function and $\delta_{\mu,\nu}$ Kronecker's delta. For a multidimensional system, such as the bead-spring polymer model, the Langevin equation is written as

$$m\ddot{\mathbf{r}}_i(t) + \gamma\dot{\mathbf{r}}_i(t) + \nabla_i E(\{\mathbf{r}_i\}) = \xi_i(t), \tag{2.3}$$

where i refers to an individual bead.

In the limit of strong coupling with the heat bath, i.e. the high friction limit, the dynamics become overdamped and are described by the Brownian equation of motion

$$\gamma\dot{\mathbf{r}}_i(t) + \nabla_i E(\{\mathbf{r}_i\}) = \xi_i(t). \tag{2.4}$$

In this limit the friction coefficient high enough such that $|\gamma \dot{\mathbf{r}}_i(t)| \gg |m\ddot{\mathbf{r}}_i(t)|$.

Since a polymer has multiple internal degrees of freedom, some collective variables need to be defined to describe the polymer. We can define the centre of mass (centroid) coordinate for a polymer with monomers having equal masses by

$$\mathbf{R}_c(t) := \frac{1}{N}\sum_{i=1}^{N} \mathbf{r}_i(t). \tag{2.5}$$

Another essential parameter is the radius of gyration $\mathbf{R}_g(t)$ defined by

$$\mathbf{R}_g^2(t) := \frac{1}{N^2}\sum_{i=1}^{N} (\mathbf{r}_i(t) - \mathbf{R}_c(t))^2. \tag{2.6}$$

Later on, the thermally averaged absolute value of $\mathbf{R}_g$ is denoted as $R_g := \sqrt{\langle \mathbf{R}_g^2 \rangle}$.

One commonly used model for polymers is the Rouse model. The Rouse model describes the polymer chain in its continuum limit and a continuous variable n is introduced to describe a position in the chain. For an ideal polymer, the harmonic potential

$$U(\{\mathbf{r}_i\}) = \sum_{i=0}^{N-1} \frac{1}{2} k_{\mathrm{harm}} (\mathbf{r}_i - \mathbf{r}_{i+1})^2, \tag{2.7}$$

couples the monomers. Using the continuum description, the following Langevin equation describing polymer dynamics in the continuum limit can be obtained [23]:

$$\gamma \frac{\partial \mathbf{r}_n(t)}{\partial t} = k_{\mathrm{harm}} \frac{\partial^2 \mathbf{r}_n(t)}{\partial n^2} + \xi_n(t). \tag{2.8}$$

The polymer has to satisfy the conditions

$$\left.\frac{\partial \mathbf{r}_n(t)}{\partial n}\right|_{n=0} = 0 \quad \text{and} \quad \left.\frac{\partial \mathbf{r}_n(t)}{\partial n}\right|_{n=N} = 0, \tag{2.9}$$

and the random force $\xi_n(t)$ the conditions

$$\langle \xi(t) \rangle = 0, \quad \text{and} \tag{2.10a}$$

$$\langle \xi_{\mu,n}(t) \xi_{\nu,m}(t') \rangle = 2\gamma k_B T \delta_{\mu,\nu} \delta(t - t') \delta(m - n). \tag{2.10b}$$

Equations (2.8), (2.9), (2.10a) and (2.10b) define the Rouse model of an ideal polymer.

To obtain a more realistic model of polymers, the excluded volume interactions are added to the chain so that beads cannot overlap. The excluded volume interactions make the chain non-ideal and the Rouse model no

longer applies. However, the scaling exponents for the radius of gyration R_g can be found for both the ideal and the non-ideal chains [23]:

$$\begin{aligned} R_g &\sim N^{1/2} \qquad \text{for ideal polymers,} \\ R_g &\sim N^{\nu} \qquad \text{for non-ideal polymers,} \end{aligned} \tag{2.11}$$

where ν is the Flory exponent. The Flory exponent in 3D is $\nu = 0.588$ ($\approx 3/5$) and in 2D $\nu = 3/4$ exactly.

Normal coordinates describing the polymer, sometimes referred to as the Rouse modes, can be obtained by a cosine-transformation using the equation [24]

$$\mathbf{X}_p(t) = \sqrt{2/N} \sum_{i=1}^{N} \mathbf{r}_i(t) \cos\left[\frac{p\pi}{N}(i - 1/2)\right], p \geq 1. \tag{2.12}$$

The zeroth Rouse mode $\mathbf{X}_0(t)$ corresponds to the centre of mass of the polymer given by Eq. (2.5) and the first $\mathbf{X}_1(t)$ describes a quantity similar to the radius of gyration by Eq. (2.6) while not being exactly the same. Using normal coordinates the autocorrelation function $C_p(t)$ can be calculated as [23]

$$C_p(t) = \langle \mathbf{X}_p(0)\mathbf{X}_p(t) \rangle = \langle \mathbf{X}_p(0)^2 \rangle \exp(-t/\tau_p), \tag{2.13}$$

where τ_p represents the relaxation (correlation) time of the pth mode, which scales with the number of monomers as [23]

$$\tau_p \sim N^{2\nu+1}. \tag{2.14}$$

The scaling law presented above can be used to determine the equilibration time of the polymer when generating uncorrelated samples from an initial distribution. These samples, used for initial configurations for molecular dynamics trajectories, can be generated by letting the system evolve according to its dynamics for a time $2\tau_p$ to make the correlations with the previous sample to decay to $1/e^2 \approx 0.1$.

The Zimm model [23] can be introduced to model hydrodynamic interactions for the polymers in a solvent. For the Zimm model with the Θ-condition satisfied (at the Θ-temperature the polymer chain becomes nearly ideal and excluded volume effects can be neglected), the Langevin equation in the continuum limit reads as

$$\frac{\partial \mathbf{r}_n(t)}{\partial t} = \sum_m \mathbf{H}_{nm} \cdot \left(k_{\text{harm}} \frac{\partial^2 \mathbf{r}_m(t)}{\partial m^2} + \xi_m(t) \right). \tag{2.15}$$

In Eq. (2.15) the mobility matrix $\mathbf{H}_{nm}$ is defined as

$$\begin{aligned} \mathbf{H}_{nn} &= \mathbf{I}/\gamma, \\ \mathbf{H}_{nm} &= \tfrac{1}{8\pi\eta|\mathbf{r}_{nm}|}[\hat{\mathbf{r}}_{nm}\hat{\mathbf{r}}_{nm} + \mathbf{I}] \qquad \text{for } n \neq m, \end{aligned} \tag{2.16}$$

where **I** is an identity matrix, η the viscosity of the solvent, $\mathbf{r}_{nm} = \mathbf{r}_n - \mathbf{r}_m$, and $\hat{\mathbf{r}}_{nm}$ is the unit vector in the direction of $\mathbf{r}_{nm}$. When the Θ-condition is satisfied the Zimm model chains act like ideal polymers and the scaling law for the diffusion coefficient of the centre of mass is $D \sim N^{-1/2}$. Due to hydrodynamic interactions in the Zimm model, outside the Θ-condition the excluded volume effects need to be taken into account and the scaling law for diffusion constant is $D \sim N^{-\nu}$. [23]

2.2 Chain models and potentials

In the work presented in this thesis, three different chain models were studied:

1. An ideal harmonic chain.

2. An ideal chain where the beads are connected by finite extension non-linear elastic (FENE) springs with Lennard-Jones (LJ) interaction between adjacent beads. This model is referred to as the ideal FENE-LJ chain.

3. A self avoiding chain where the beads are connected with FENE springs and LJ interaction is between all the beads. This model is referred to as the self-avoiding FENE-LJ chain.

The simplest chain model studied was a discrete ideal harmonic chain, where the beads with no excluded volume interaction are connected with harmonic springs given by Eq. (2.7). This model will be referred as an ideal harmonic chain.

A more 'realistic' chain is modelled using FENE springs accompanied with a truncated LJ potential. This FENE-LJ model consist of the interaction potential

$$U(\{\mathbf{r}_i\}) = \sum_{i}^{N-1} U_{\mathrm{FENE}}(|\mathbf{r}_i - \mathbf{r}_{i+1}|) + \sum_{\langle i,j \rangle}^{N} U_{\mathrm{LJ}}(|\mathbf{r}_i - \mathbf{r}_j|), \tag{2.17}$$

where

$$U_{\mathrm{FENE}}(r) = -\frac{1}{2} k_F R_0^2 \ \ln(1 - r^2/R_0^2), \tag{2.18}$$

and

$$U_{\mathrm{LJ}}(r) = 4\epsilon[(\sigma/r)^{12} - (\sigma/r)^6 + 1/4]. \tag{2.19}$$

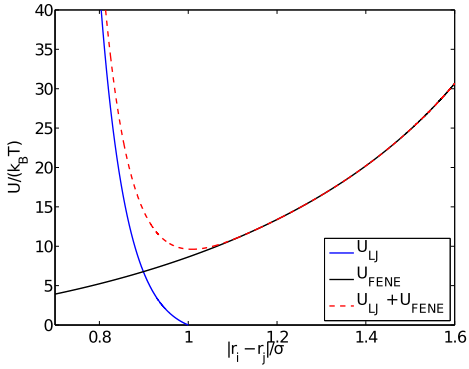

Figure 2.2. The FENE-LJ interaction potential between adjacent beads, see Eq. (2.17). The LJ potential acts between all the beads in the self-avoiding chain model but only between consecutive beads in the ideal chain model. The U_{FENE} component of the potential diverges at $R_0 = 2.0$, setting a maximum in the separation between consecutive beads.

Above, k_{FENE} is the FENE spring constant, R_0 gives the maximum separation of the adjacent beads. In the LJ potential, σ is the radius of the excluded volume, and ϵ the energy parameter. The repulsive interaction between the beads is a LJ potential that is truncated and shifted so that $U_{LJ}(r) = 0$ if $r > 2^{1/6}\sigma$. The shift by ϵ ensures continuity of the function. The FENE-LJ interaction potential between adjacent beads is illustrated in Fig. 2.2. When the second summation in Eq. (2.17) is carried out over all the pairs, the model will be referred to as the self-avoiding FENE-LJ chain. When the summation is only over adjacent beads, the model is referred to as the ideal FENE-LJ chain.

Polymer escape was studied in two different external potentials: a one-dimensional potential shown in the left panel of Fig. 2.3, and a two-dimensional potential shown in the right panel of Fig. 2.3. The one-dimensional external potential is a quartic double well with the function

$$V(x) = -\frac{\omega^2}{2}x^2 + \frac{\omega^2}{4a_0^2}x^4, \tag{2.20}$$

where $\pm a_0$ gives the location of the minima, the energy has a maximum at $x = 0$, and ω^2 is the curvature of the energy barrier. The same external potential with Brownian dynamics for ideal harmonic polymers was used in Ref. 15.

The two-dimensional external potential with confinement in the y-direction is

$$V(x,y) \quad = \quad \begin{cases} \frac{1}{2}\omega_0^2(x^2+y^2), & x \le x_0; \\ \Delta V - \frac{1}{2}\omega_b^2(x-x_b)^2 + \frac{1}{2}\omega_0^2 y^2, & x > x_0; \end{cases} \tag{2.21}$$

where the quantities ω_0 and ω_b give the curvature of the well and of the barrier, respectively, ΔV is the height of the barrier located at x_b and x_0 the cross-over point between the two parabolas. A potential function with the same x-dependence but without confinement in the y-direction was used in the work of Shin *et al.* [18] and was compared in the work presented in this thesis. The two-dimensional external potential without confinement in the y-direction is

$$V(x,y) = \begin{cases} \frac{1}{2}\omega_0^2 x^2, & x \leq x_0; \\ \Delta V - \frac{1}{2}\omega_b^2 (x - x_b)^2, & x > x_0. \end{cases} \tag{2.22}$$

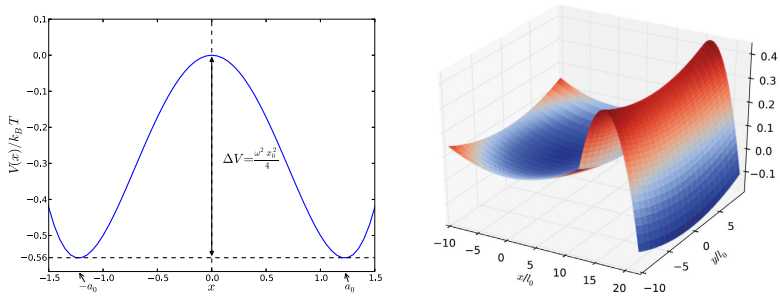

Figure 2.3. left: The one-dimensional external potential of Eq. (2.20). right: The two-dimensional external potential of Eq. (2.21).

2.3 Rate theories

As a rare event, polymer escape is often computationally too expensive to be numerically solved by 'brute-force' simulations. Section 3.1 describes the molecular dynamics (MD) methodology to simulate the escape rate directly. However, there is a separation of time scales in the problem: internal vibrations which need to be sampled in MD are orders of magnitude faster than an actual escape event. When sampling the MD trajectories, the system spends most of the simulation time in the initial minimum and rarely escapes over the energy barrier. This leads to inefficient sampling of the escape events.

To overcome this problem rate theories are introduced. In rate theories, the escape rate is solved using a toolkit from statistical mechanics and there is no need to sample long time scale trajectories. This section describes two commonly used rate theories: the harmonic transition state theory and Langer's theory.

2.3.1 Harmonic transition state theory

In transition state theory (TST) the phase space of the system is divided by the transition state (TS) hyperplane into the initial (I) and the final states (F) (reactant and product states in the original context) [25, 26]. The escape rate is then given by

$$\mathcal{R}_{\mathrm{TST}} = \mathrm{Prob}(\text{'system in TS'}) \times \text{'flux out of TS'}. \tag{2.23}$$

The probability that system reaches the transition state from the initial state can be estimated by the fraction of the configuration integrals $Z_{\mathrm{TS}}/Z_{\mathrm{I}}$, where Z_{I} is the configuration integral over I, and Z_{TS} is the configuration integral over TS. The flux out of TS can be computed analytically and it is the average of the equilibrium velocity perpendicular to the TS hyperplane at the TS $\langle v_\perp \rangle = \sqrt{k_B T/(2\pi\mu_\perp)}$, where $\mu_\perp$ is the reduced mass for the perpendicular component of the system. Thus, the TST rate expression becomes

$$\mathcal{R}_{\mathrm{TST}} = \sqrt{\frac{k_B T}{2\pi\mu_\perp}} \frac{Z_{\mathrm{TS}}}{Z_{\mathrm{I}}}. \tag{2.24}$$

The four assumptions made in TST are

1. The Born-Oppenheimer approximation.

2. Classical dynamics of nuclei.

3. Boltzmann distribution in initial state.

4. No recrossings of TS.

The first two assumption are clearly met for the coarse-grained polymer model in the temperature range studied. The third assumption is satisfied when the energy barrier of the escape is high enough, roughly $\Delta E > 5k_B T$. For the current problem, the last assumption is generally not met. Keck has shown that the effect of recrossings can be minimised by variationally optimising the transition state dividing surface [27]. Also, dynamical corrections to TST can be calculated with various methods to estimate the effect of recrossing trajectories [28, 29]. Two methods for computing the dynamical correction factor are explained in Secs. 2.3.2 and 3.4.1.

Instead of full numerical sampling, the configuration integrals Z_{TS} and

Z_{I} can be computed with a harmonic approximation of the potential energy [30, 31]. The maximum energy along the minimum energy path (MEP) from I to F is a saddle point (‡) which represents the bottleneck for the transition. The rate expression of the harmonic transition state theory (HTST) is

$$\mathcal{R}_{\mathrm{HTST}} = \frac{1}{2\pi\sqrt{\mu_\perp}} \sqrt{\frac{\prod_{i=1}^{N} \lambda_i^0}{\prod_{i=2}^{N} \lambda_i^\ddagger}} e^{-\Delta E/k_B T}, \tag{2.25}$$

where ΔE is the height of the energy barrier along the MEP, λ_i^0 and $\lambda_i^\ddagger$ are the eigenvalues of Hessian matrices $\mathbf{H}_0$ and $\mathbf{H}_\ddagger$ at the initial minimum and at the saddle point, respectively. The elements of the Hessian matrix $\mathbf{H}_p$ are given by

$$(H_p)_{ij} = \left. \frac{\partial^2 E(\mathbf{r})}{\partial r_i \partial r_j} \right|_{\mathbf{r}=\mathbf{r}_p}, \tag{2.26}$$

where p refers to a point on the MEP.

For the polymer escape problem in the external potential of Eq. (2.20), it is known that short ideal chains cross the barrier in a coiled state when polymer length is below the critical length: $N < N_C$. Above N_C the polymer is in a stretched state at the barrier top. Lee and Sung [15] have derived an analytical expression for N_C using a continuum chain model:

$$N_C = \sqrt{\frac{K\pi^2}{\omega^2}}. \tag{2.27}$$

At N_C the eigenvalue of the second lowest eigenmode at the saddle point $\lambda_2^\ddagger$ approaches zero and therefore causes a divergence in the escape rate. The anharmonic corrections to this mode can be introduced to reduce this divergence

$$g(\alpha) = \sqrt{\frac{\alpha}{2\pi}} \int_{-\infty}^{\infty} dQ e^{-(\alpha/2)Q^2 - (3/8)Q^4}, \tag{2.28}$$

where $\alpha = \lambda_2^\ddagger a_0 \sqrt{N/(k_B T)}/\omega$ [15]. Thus, the corrected HTST rate becomes

$$\mathcal{R}_{\mathrm{HTST+AHC}} = g(\alpha)\mathcal{R}_{\mathrm{HTST}}. \tag{2.29}$$

2.3.2 Dynamical corrections

The assumption of no recrossings of the TS in TST is often not satisfied for energy barriers that are flat. The effect of the recrossings can, however, be estimated using calculations of classical trajectories started at the TS. This provides dynamical corrections (DC) to the TST rate estimate. The

correction factor, κ, is [29]:

$$\kappa = \frac{2}{N_{\mathrm{traj}}} \sum_{i=1}^{N_{\mathrm{traj}}} \mathrm{sgn}(v_i)\theta(X_0^{\mathrm{final}}), \tag{2.30}$$

where $\mathrm{sgn}(v_i)$ is the sign of the initial net velocity $v_i = \sum_{j=1}^{N} v_j$ of a trajectory i assigned from the Maxwell-Boltzmann distribution $P(v) \propto \exp[-v^2/(2k_BT)]$, and $\theta(X_0^{\mathrm{final}})$ is unity if the system resides in F at the end of the trajectory and zero otherwise. Thus, each trajectory that ends in F, contributes positively to κ if it starts with a velocity pointing towards F, but contributes negatively if the initial velocity points towards I. Trajectories ending in I do not contribute to κ. The corrected rate estimate is

$$\mathcal{R}_{\text{HTST+AHC+DC}} = \kappa \mathcal{R}_{\text{HTST+AHC}}, \tag{2.31}$$

where $\mathcal{R}_{\text{HTST+AHC}}$ is given by Eq. (2.29). While direct dynamical calculations of transitions can be impossibly long for systems with low transition rates, the calculation of DC requires only short trajectories and can be carried out with much less computational effort.

2.3.3 Kramers' and Langer's rate theory

Kramers' rate theory gives the escape rate for a particle from a one-dimensional potential well by thermal activation [8, 32]. In the moderate-to-strong friction regime the expression for the rate is

$$\mathcal{R}_{\mathrm{K}} = \left[\left(\frac{\gamma^2}{4} + \omega_B^2 \right)^{\frac{1}{2}} - \frac{\gamma}{2} \right] \frac{\omega_0}{2\pi\omega_B} e^{\Delta E/k_BT}, \tag{2.32}$$

where ω_B is the curvature at the barrier top, ω_0 the curvature at the initial minimum, ΔE the height of the potential energy barrier, and γ the friction coefficient. For the strong friction regime $\gamma \gg \omega_B$, the overdamped limit, the Eq. (2.32) simplifies to

$$\mathcal{R}_{\mathrm{K}} = \frac{\omega_0\omega_B}{2\pi\gamma} e^{\Delta E/k_BT}. \tag{2.33}$$

The escape rate for a multidimensional system is derived by Langer in the overdamped limit [9]. In general form, the expression for the rate is [15]

$$\mathcal{R}_{\mathrm{L}} = \frac{\omega_B}{2\pi\gamma} \frac{Z_{\ddagger}}{Z_0} \sqrt{2\pi k_BT} e^{-\Delta E/k_BT}, \tag{2.34}$$

where $Z_{\ddagger}$ and Z_0 are the partition functions near the saddle point and near the initial minimum. Using the harmonic approximation, the partition

functions can be evaluated to obtain

$$\mathcal{R}_{\mathrm{L}} = \frac{\sqrt{|\lambda_1^\ddagger|}}{2\pi\gamma} \sqrt{\frac{\prod_{i=1}^{N} \lambda_i^0}{\prod_{i=2}^{N} \lambda_i^\ddagger}} e^{-\Delta E/k_B T}, \tag{2.35}$$

where λ_i^0 and $\lambda_i^\ddagger$ are the eigenvalues of Hessian matrix of Eq. (2.26), and the eigenvalue of the unstable mode $\sqrt{|\lambda_1^\ddagger|}$ is taken to represent the curvature at the barrier top. The rate resembles the HTST expression of Eq. (2.25) but it is derived from different assumptions. The derivation of Langer's equation (2.35) follows the same steps as Kramer's equation (2.33). In Kramers' and Langer's theory, a harmonic approximation is made also along the MEP, while in HTST the harmonic approximation is only made for directions perpendicular to the MEP.

3. Numerical methods

3.1 Molecular dynamics

The most straightforward way to calculate the escape rate is to use molecular dynamics (MD). Within MD, the equations of motion are numerically integrated to generate trajectories representing transitions from the initial state (I) to the final state (F). The dynamics of the system can be described either by the Langevin Eq. (2.3) or the Brownian Eq. (2.4).

In MD, a polymer is initially placed in I and let to reach thermal equilibrium for a time interval twice as long as the correlation time τ. The correlation time scales with the polymer length as $\tau \propto N^{2\nu+1}$ [23]. For ideal chains $\nu = 1/2$ and for self-avoiding chains in two-dimensions $\nu = 3/4$. Equilibration in the initial state ensures the generation of uncorrelated samples from the Boltzmann distribution $P_{\mathrm{I}}(\mathbf{r}) \propto \exp(-E(\mathbf{r})/k_B T)$. During the equilibration the polymer is confined to the initial state by a reflecting wall at the barrier top.

For trajectories from I to F, the escape probability can be determined as

$$P_{\mathrm{esc}}(t) = (1/N_{\mathrm{traj}}) \sum_{i=1}^{N_{\mathrm{traj}}} \theta(t - t_i), \tag{3.1}$$

where N_{traj} is the number of simulated trajectories, $\theta(t-t_i)$ the Heaviside step function and t_i the time of the ith escape event. An escape event is considered to have occurred when the centre of mass of the system X_0 has reached a predefined threshold value. Usually a value larger than the barrier width is used so that the system is unlikely to return to I. The dynamical escape rate is given by

$$\mathcal{R}_{\mathrm{MD}} = \frac{dP_{\mathrm{esc}}(t)}{dt} \,, \tag{3.2}$$

where the derivative is computed by fitting the curve $P_{\mathrm{esc}} = \mathcal{R}_{\mathrm{MD}} t + b$,

where b is a constant, over the time interval where $P_{\mathrm{esc}}(t)$ is close to being a linear function of t. The error $\Delta\mathcal{R}_{\mathrm{MD}}$ is estimated as the standard deviation of the derivative $dP_{\mathrm{esc}}(t)/dt$ in the fitting interval divided by $\sqrt{N_s}$, where N_s is the number of data points in the fitting interval. The average time in between the escape events is $t_{\mathrm{esc}} = \langle t_i \rangle = (1/N_{\mathrm{traj}}) \sum_{i=1}^{N_{\mathrm{traj}}} t_i$.

Equation (2.3) describing Langevin dynamics is numerically integrated using the Brünger-Brooks-Karplus (BBK) integration scheme [33, 34]. The integrator reads as

$$\mathbf{v}(t_n + \frac{1}{2}\delta t) = (1 - \frac{1}{2}\gamma\delta t)\mathbf{v}(t_n) + \frac{1}{2m}[-\mathbf{F}(\mathbf{r}(t_n)) + \xi(t_n)]\delta t; \tag{3.3a}$$

$$\mathbf{r}(t_n + \delta t) = \mathbf{r}(t_n) + \mathbf{v}(t_n + \frac{1}{2}\delta t)\delta t; \tag{3.3b}$$

$$\mathbf{v}(t_n + \delta t) = \frac{\mathbf{v}(t_n + \frac{1}{2}\delta t) + \frac{1}{2}m[-\mathbf{F}(\mathbf{r}(t_n + \delta t)) + \xi(t_n + \delta t)]\delta t}{1 + \frac{1}{2}\gamma\delta t} \tag{3.3c}$$

where δt is the time step, and $\mathbf{F}(\mathbf{r}(t_n)) + \xi(t_n)$ the net force of the system at time t_n. Equation (2.4) describing Brownian dynamics is integrated with the forward Euler method

$$\mathbf{r}(t_n + \delta t) = \mathbf{r}(t_n) + \frac{\delta t}{\gamma}[-\mathbf{F}(\mathbf{r}(t_n)) + \xi(t_n)]. \tag{3.4}$$

3.2 Path integral hyperdynamics

The Path Integral Hyperdynamics (PIHD) method is a reweighting scheme in which the external potential is modified to accelerate the simulations [35]. The escape rate is computed in a modified external potential where the escape events are more frequent and the escape rate in the original potential is obtained by reweighting the trajectories simulated in the modified potential. In addition to the polymer escape problem [18] PIHD has been applied to adatom diffusion in a periodic potential and shown to work even with a time-dependent bias force [36]. In this section we explain the idea of PIHD in one particle case and present a way of computing the escape rate for multidimensional systems.

3.2.1 One degree of freedom

The probability of finding a particle at position r_f at time t_f, given it has been at r_0 at time t_0, is

$$P(r_0, t_0 | r_f, t_f) = C \int [Dr] \exp(-\beta I[r(t)]), \tag{3.5}$$

where C is a normalisation constant and $[Dr]$ presents integration over all possible trajectories $r(t)$. Each trajectory $r(t)$ has an action

$$I[r(t)] = \frac{1}{4\gamma}\int_{t_0}^{t_f} dt'[m\ddot{r}(t') + \gamma\dot{r}(t') + \nabla V(r)]^2, \tag{3.6}$$

where $V(r)$ is the external potential of the system. In the PIHD method the external potential is modified by a bias potential $V_{\text{bias}}(r)$ resulting in a boosted potential $V_b(r) = V(r) + V_{\text{bias}}(r)$. The action $I[r(t)]$ is then written in terms of the boosted potential and algebraically modified into two parts as

$$\begin{aligned} I[r(t)] &= \frac{1}{4\gamma}\int_{t_0}^{t} dt'[m\ddot{r}(t') + \gamma\dot{r}(t') + \nabla V_b(r) - \nabla V_{\text{bias}}(r)]^2 \\ &= \underbrace{\frac{1}{4\gamma}\int_{t_0}^{t} dt'[m\ddot{r}(t') + \gamma\dot{r}(t') + \nabla V_b(r)]^2}_{=I_b[r(t)]} \\ &\quad + \underbrace{\frac{1}{4\gamma}\int_{t_0}^{t} dt'[\nabla V_{\text{bias}}(r)^2 - 2\xi(t')\nabla V_{\text{bias}}(r)]}_{=I_\xi[r(t)]} \qquad (3.7) \\ &= I_b[r(t)] + I_\xi[r(t)], \qquad (3.8) \end{aligned}$$

where $\xi(t')$ comes from Eq. (2.2). Now Eq. (3.5) can be written as

$$P(r_0, t_0|r_f, t_f) = C\int [Dr]\exp(-\beta I_b[r(t)])\exp(-\beta I_\xi[r(t)]). \tag{3.9}$$

An escape event is considered to occur when a particle leaves the initial state I and enters the final state F defined as $r \geq r'$. The probability for an escape event is

$$P_{\text{esc}}(t) = \int_{r\geq r'} dr \int_{r_0<r'} dr_0 P(r_0)P(r_0, t_0|r, t), \tag{3.10}$$

where the first integration is over the final state F and the second integration is over the initial state I. $P(r_0)$ is the equilibrium distribution of the initial configurations. In the numerical simulations, integration over the equilibrium distribution is handled by letting the system equilibrate in the initial state. The integration over the final state is numerically computed by sampling the trajectories initiated from I and ending in F. Thus, the escape probability of Eq. (3.10) can be written in the sampling form

$$P_{\text{esc}}(t) = \frac{1}{\mathcal{N}_\xi}\sum_{i=1}^{N_{\text{traj}}} \theta(t - t_i)\exp(-\beta I_\xi[r_i(t)]), \tag{3.11}$$

where t_i is the time of an escape event, $\theta(\dots)$ the Heaviside step function, and $\exp(-\beta I_\xi[r_i(t)])$ a PIHD weight assigned to each trajectory. The

normalisation factor $\mathcal{N}_\xi$ is computed as

$$\mathcal{N}_\xi = \sum_{i=1}^{N_{\text{traj}}} \exp(-\beta I_\xi[r_i(t)]). \tag{3.12}$$

The action $I_\xi[r(t)]$ is numerically integrated during the simulation as

$$I_\xi[r(t)] = \frac{1}{4\gamma}\int_{t_0}^{t} dt' \nabla V_{\text{bias}}(r)[\nabla V_{\text{bias}}(r) - 2\xi(t')]. \tag{3.13}$$

3.2.2 Multiple degrees of freedom

In a multidimensional system the action $I_\xi[r(t)]$ of Eq. (3.13) is computed individually for each degree of freedom

$$I_{i,\xi[r_i(t)]} = \frac{1}{4\gamma}\int_{t_0}^{t} dt' \nabla_i V_{\text{bias}}(\mathbf{r}_i)\cdot[\nabla_i V_{\text{bias}}(\mathbf{r}_i) - 2\xi_i(t')]. \tag{3.14}$$

The net action $I_\xi[r(t)]$ is then a sum over the individual degrees of freedom

$$I_{\xi[r(t)]} = \sum_{i=1}^{N} I_{i,\xi[r(t)]} = \frac{1}{4\gamma}\sum_{i=1}^{N}\int_{t_0}^{t} dt' \nabla_i V_{\text{bias}}(\mathbf{r}_i)\cdot[\nabla_i V_{\text{bias}}(\mathbf{r}_i) - 2\xi_i(t')]. \tag{3.15}$$

The integral over time can be computed in a discrete form as

$$I_{\xi[r(t)]} = \frac{1}{4\gamma}\sum_{i=1}^{N}\sum_{t_k=0}^{t_k=t} \nabla_i V_{\text{bias}}(\mathbf{r}_{i,k}))\cdot[\nabla_i V_{\text{bias}}(\mathbf{r}_{i,k})) - 2\xi_{i,k}]\delta t, \tag{3.16}$$

where k referers to discretised time and δt is the time step. The normalisation factor for a multidimensional system is

$$\mathcal{N}_\xi = \sum_{j=1}^{N_{\text{traj}}}\sum_{i=1}^{N} e^{-\beta I_i[\mathbf{r}_j(t)]}. \tag{3.17}$$

The effect of PIHD on the escape probability curve is shown in Fig. 3.1. PIHD smoothens the escape probability curve thus reducing the variance in the fitted line whose tangent is the escape rate $\mathcal{R}$.

3.2.3 Bias potential

The bias potential for each bead was chosen here to be

$$V_{\text{bias}}(x,y) \;=\; \begin{cases} -\frac{1}{2}b\omega_0^2 x^2, & x \le x_0; \\ -b\Delta V + \frac{1}{2}b\omega_b^2(x-x_b)^2, & x > x_0. \end{cases} \tag{3.18}$$

where b is a parameter to be chosen between $0 \le b < 1$. Thus the bias potential flattens the external potential along the x-axis making escape events more frequent. We tried a few different choices of the bias potential, including a constant force on all the beads as well as dragging the chain from one end. The one described by Eq. (3.18) here worked best.

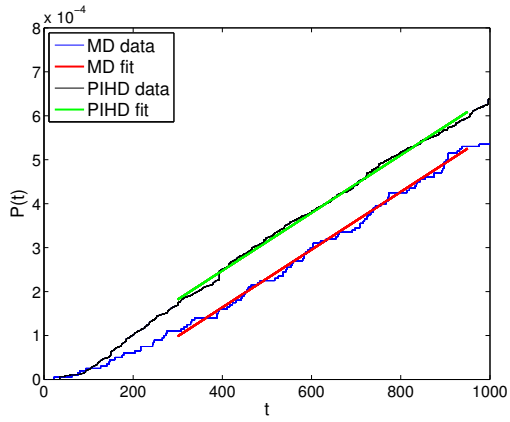

Figure 3.1. The escape probability for a self-avoiding chain of length $N = 32$ using MD and PIHD and corresponding linear fits to obtain the escape rate. The figure shows that the PIHD smoothens the escape curve therefore improving the accuracy of the estimate for the escape rate.

3.3 Nudged elastic band

In order to apply the harmonic transition state theory (HTST) of Eq. (2.25) in the one-dimensional external double well potential of Eq. (2.20), the saddle point of transition (‡) and the initial minimum need to be known. To find the saddle point, the minimum energy path (MEP) from I to F is computed using the Nudged Elastic Band (NEB) method [37, 38, 39] in the external potential of Eq. (2.20). In the NEB method, a set of replicas of the system, referred to as images, $\{\mathbf{r}_p\}_{p=1}^{P}$ are placed along a path between the initial state minimum $\mathbf{r}_{\mathrm{I}} = -a_0\mathbf{1}$ and the final state minimum $\mathbf{r}_{\mathrm{F}} = a_0\mathbf{1}$, where $=[1, 1, \ldots, 1]$ is a vector of length equal to the polymer length N.

The images represent a discretisation of the path and to control the distribution of these discretisation points, the images are connected with harmonic springs with spring constant k_{NEB}. An estimate of the tangent [37] to the path is used to project out the parallel component of the true force acting on the beads and the perpendicular component of the spring force (the 'nudging'). The images are then displaced iteratively using Velocity Verlet integration with velocity projection so as to zero the net force acting on the beads until the images lie along the MEP.

At the end of the NEB calculation the images give a discrete representation of the MEP, but no image will be exactly at the saddle point. An accurate estimate of the saddle point was found here by identifying the image with the highest energy and then minimising the force on this im-

age with the Newton-Raphson method. The method consists of iterations $\mathbf{r}^{(n+1)} = \mathbf{r}^{(n)} - \mathbf{H}^{-1}\mathbf{F}^{\mathrm{sys}}(\mathbf{r}^{(n)})$, where $\mathbf{F}^{\mathrm{sys}}(\mathbf{r})$ is the force of the real system (no NEB spring forces) and $\mathbf{H}^{-1}$ is an inverse of the Hessian matrix (Jacobian matrix of the force) with elements given by Eq. (2.26). Within a few iterations, the method converges to a point $\mathbf{r}_\ddagger$ where $\mathbf{F}(\mathbf{r}_\ddagger) = 0$. If the initial point is close enough to a saddle point, then the Newton-Raphson method will most likely converge into the saddle point rather than other points where the force is zero. The activation energy is then given by the energy difference between the initial state and the saddle point as $\Delta E = E(\mathbf{r}_\ddagger) - E(\mathbf{r}_0)$. The Hessian matrices $\mathbf{H}_0$ and $\mathbf{H}_\ddagger$ of Eq. (2.26) are evaluated using the finite difference method.

3.4 Forward flux sampling

The forward flux sampling (FFS) method was initially developed to study rare events in non-equilibrium systems with stochastic dynamics [40, 41, 42, 43]. FFS is generally speaking a class of methods based on a series of interfaces, or planes, between the initial and final states. A rare event transition from the initial state to the final state is described by the order parameter λ which is used to define the initial and final states. A series of interfaces $\lambda_0, \lambda_1, \ldots, \lambda_n$ is then placed between the initial and final states. The rate constant is computed by sampling the dynamics between these interfaces.

Using FFS, the rate constant is obtained as [41]

$$\mathcal{R}_{\mathrm{FFS}} = \frac{\bar{\Phi}_{I,0}}{\bar{h}_I} P(\lambda_n, \lambda_0), \tag{3.19}$$

where $\bar{\Phi}_{I,0}/\bar{h}_I$ is the initial flux across the first plane λ_0 towards the final state and $P(\lambda_n|\lambda_0)$ is the probability for the system to reach the plane λ_n given it was initially at λ_0. In the current work the 'direct' FFS method was used to obtain the escape rate of a polymer in the external symmetric double well potential. The following procedure describes the 'direct' FFS algorithm.

1. The initial flux is calculated by running a long trajectory in the initial state for time t_{init} and counting the number of crossings q of the first interface λ_0 towards the final state. Therefore, the initial flux is $\bar{\Phi}_{I,0}/\bar{h}_I = q/t_{\mathrm{init}}$.

2. A configuration is picked up randomly from the initial configurations generated and a trajectory starting from this configuration is simulated until λ_1 is reached or until the trajectory returns to the initial state by crossing λ_0. Each successful crossing of λ_1 is stored. The probability $P(\lambda_1|\lambda_0)$ is then estimated as a fraction between the number of successful crossings and the number of all trajectories.

3. The previous step is repeated using the end points of the successful trajectories at λ_1 as initial configurations. The trajectories are simulated until λ_2 is reached or until the trajectory returns to the initial state by crossing λ_0. The probability $P(\lambda_2|\lambda_1)$ is estimated again as a fraction between the number of successful crossings and the number of all trajectories.

4. The procedure is repeated until λ_n is reached and the probability $P(\lambda_n|\lambda_0)$ can be computed as

$$P(\lambda_n|\lambda_0) = \prod_{i=0}^{n-1} P(\lambda_{i+1}|\lambda_i). \tag{3.20}$$

A Gaussian statistical error estimate for the rate is obtained by repeating the FFS calculation several times.

The most straightforward way to position the planes is to place them between the initial and final states with equal spacing. The computational efficiency of the 'direct' FFS method can be optimised by adjusting the plane positions [42, 44]. The planes are adjusted in a way that the flux $P(\lambda_{i+1}|\lambda_i)$ across the planes stays as constant as possible. Additional planes are added to the region where the flux is small and planes are removed from where the flux is large.

3.4.1 Dynamical corrections using forward flux sampling

The computation of the dynamical correction factor κ for transition state theory was presented in Sec. 2.3.2. In this thesis we studied an alternative way of computing the dynamical correction factor κ using FFS. Instead of placing the first plane near the initial state we place the first plane at the barrier top where the centre of mass of the polymer is exactly at the barrier top. The last plane is placed near the final minimum.

In the computation of κ, the initialisation is done by simulating the polymer confined into the initial hyperplane at the barrier top. At each

time step, the net force is reduced from each bead as $F_i - 1/N \sum_{i=1}^{N} F_i$, so that the centre of mass of the polymer stays in the hyperplane. Uncorrelated initial configurations in the hyperplane are generated by letting the polymer relax twice the correlation time τ while confined on the hyperplane. For each initial configuration generated, a random velocity from the Maxwellian distribution $P(v_i) \propto \exp(-mv_i^2/2)$ is assigned to each degree of freedom i. If the net velocity of the polymer $\sum_{i=1}^{N} v_i$ is negative the velocities of individual beads are reversed as $v_i \to -v_i$. This ensures that the samples generated present trajectories crossing the hyperplane to the direction of the final state.

Using these initial configurations, the forward flux to the final state is computed according to Eq. (3.20). The expression for κ is then

$$\kappa = P(\lambda_n|\lambda_0) = \prod_{i=0}^{n-1} P(\lambda_{i+1}|\lambda_i). \tag{3.21}$$

3.5 Effective potentials

The escape rate of the multidimensional polymer system can also be estimated with one-dimensional Kramers' Eq. (2.33) when the multidimensional energy landscape is coarse-grained into a single reaction coordinate. One possibility is to choose the x-coordinate of the centre of mass x_C as the independent variable. An effective potential energy curve for this one degree of freedom is then obtained by thermally averaging over all the other degrees of freedom. The thermal average of a function $f(\mathbf{r})$ for a fixed value of the x-coordinate of the centre of mass is

$$\langle f \rangle_{\mathrm{C}} = \frac{1}{Z_N(x_{\mathrm{C}})} \int \prod_{i=1}^{N} d\mathbf{r}_i' f(\{\mathbf{r}_i'\}) \delta(x_{\mathrm{C}} - \underbrace{\frac{1}{N}\sum_{j=1}^{N} x_j'}_{=x_{\mathrm{C}}'}) e^{-\beta E(\{\mathbf{r}_i'\})}, \tag{3.22}$$

where

$$Z_N(x_{\mathrm{C}}) = \int \prod_{i=1}^{N} d\mathbf{r}_i' \delta(x_{\mathrm{C}} - \frac{1}{N}\sum_{j=1}^{N} x_j') e^{-\beta E(\{\mathbf{r}_i'\})}. \tag{3.23}$$

By applying this averaging to the total potential energy, an effective energy curve $E_{\mathrm{eff}}(x_{\mathrm{C}}, N) = \langle E \rangle_{\mathrm{C}}$ is obtained. The friction coefficient for this reduced dimensionality system is $\gamma_{\mathrm{eff}} \approx N\gamma_K$. The effective friction coefficient in the Kramers rate expression, γ_K, was adjusted here to obtain a good estimate of the simulated escape rate of a single particle and turned out to be $\gamma_K = 0.82\gamma$ in the two-dimensional external potential of

Eq. (2.21). The Kramers approximation for the escape rate of a polymer with N beads is thus obtained as

$$\mathcal{R}_{\mathrm{K}}(N) = \frac{\omega_{0,\mathrm{eff}}(N)\omega_{B,\mathrm{eff}}(N)}{2\pi\gamma_{\mathrm{eff}}} e^{-\beta\Delta E_{\mathrm{eff}}(N)}. \tag{3.24}$$

From the shape of the effective potential curves, the parameters $\omega_{0,\mathrm{eff}}(N)$, $\omega_{B,\mathrm{eff}}(N)$ and $\Delta E_{\mathrm{eff}}(N)$ were estimated by fitting parabolas at the initial state minimum and at the barrier maximum.

The internal degrees of freedom of the polymer contribute to the effective potential curve E_{eff}. Alternatively, an effective external potential curve without including the interaction between the beads can be calculated as $V_{\mathrm{eff}}(x_{\mathrm{C}}, N) = \langle V_{\mathrm{ext}} \rangle_{\mathrm{C}}$. We compare the two energy curves and the Kramers rate estimates obtained from each one in Sec. 4.1.

More accurately, a two-dimensional energy surface can be sampled by thermal averaging with the reaction coordinate defined as (x_c, R_g), where R_g is the radius of gyration. The thermal average for a two-dimensional reaction coordinate is

$$\langle f \rangle_{\mathrm{C},R_g} = \frac{1}{Z_N(x_{\mathrm{C}}, R_g)} \int \prod_{i=1}^{N} d\mathbf{r}_i' f(\{\mathbf{r}_i'\}) \delta(R_g - R_g') \delta(x_{\mathrm{C}} - x_{\mathrm{C}}') e^{-\beta E(\{\mathbf{r}_i'\})}, \tag{3.25}$$

where

$$Z_N(x_{\mathrm{C}}, R_g) = \int \prod_{i=1}^{N} d\mathbf{r}_i' \delta(R_g - R_g') \delta(x_{\mathrm{C}} - x_{\mathrm{C}}') e^{-\beta E(\{\mathbf{r}_i'\})}. \tag{3.26}$$

Equation (3.25) can be used to sample the two-dimensional total potential energy surfaces $E_{\mathrm{eff}}(x_{\mathrm{C}}, R_g, N) = \langle E \rangle_{\mathrm{C},R_g}$ of escape events.

4. Results

4.1 Escape in an asymmetric potential well

In Publication I, the escape rates of ideal and self-avoiding FENE chains were studied in the two-dimensional system. Two variants of the external potential were used: the external potential of Eq. (2.21) with a confinement in the y-direction and the external potential of Eq. (2.22) without a confinement in the y-direction. The external potential without the y-directional confinement has been previously considered by Shin *et al.* [18]. The escape rate was solved with the path integral hyperdynamics (PIHD) simulations and with Kramers' Eq. (3.24) using effective potentials. Chain lengths studied were $N = \{8, 16, \ldots, 80\}$.

The values of the parameters used in the simulations were $m = m_0 = 1870$ amu, $k_BT = 1.2$ and $\sigma = 1.02$ nm, which roughly correspond to three base pairs of double stranded DNA. These parameters fix the mass, length and energy scales resulting in a time scale characteristic of the LJ potential as $t_{\mathrm{LJ}} = \sqrt{m\sigma^2/\epsilon} = 30.9$ ps, where $\epsilon = 1\ k_BT$. The external potential was defined by parameters $\omega_0 = 0.0014$, $\omega_b = 0.032$, $\Delta V = 0.3\ k_BT$. The barrier was located at position $x_b = 16$ and the crossover between the two parabolas at $x_0 = 12$. The parameter in the FENE spring constant was $k_F = 15$ and the maximum FENE separation $R_0 = 2.0$. The Langevin equation was integrated in time using the BBK integration scheme of Eq. (3.3) with a time step of $\delta t = 0.005$. The BBK-integrator is particularly well suited for PIHD. The criterion for a crossing event in the PIHD simulations was that the x-coordinate of the centre of mass x_{C} has reached $x_b + 4.0$. The PIHD bias parameter b in Eq. (3.18) was chosen between $0.7 \ldots 0.9$. The effective potential curves Φ_{eff} and V_{eff} were sampled holding the centre of the mass of the system still at a given position x_C while

the samples were generated.

The friction chosen in the Langevin dynamics, $\gamma = 0.7$ ($= 3.8 \times 10^{-6}$ kg/s), corresponds to the high friction range of Kramers' theory $\gamma \gg \pi\omega_b$ [8]. With this choice of friction, the effective viscosity of the fluid surrounding the polymer can be estimated to be $\eta \approx 1.3 \times 10^{-5}$ g(cm s)$^{-1}$ (for water $\eta = 1$ g (cm s)$^{-1}$) [22].

4.1.1 Effect of confining external potential

The escape rates for a self-avoiding chain from both external potentials, with the y-directional confinement of Eq. (2.21) and without the y-directional confinement Eq. (2.22), are shown in Fig. 4.1. With both external potentials the escape rate has a minimum around $N = 32$, after which the escape rate starts to increase. This increase is larger when the confinement in the y-direction is present. This is due to 'crowding' in the potential well; with the confining external potential, the long polymers no longer fit in the potential well and obtain a higher potential energy at the minimum. The effective potentials at the minimum $V_{\text{eff}}(0, N)$ and at the barrier top $V_{\text{eff}}(x_b, N)$ are shown in Fig. 4.2. The potential energy at the minimum increases faster when the y-directional confinement is present. This lowers the energy barrier of the escape thus enhancing the escape rate.

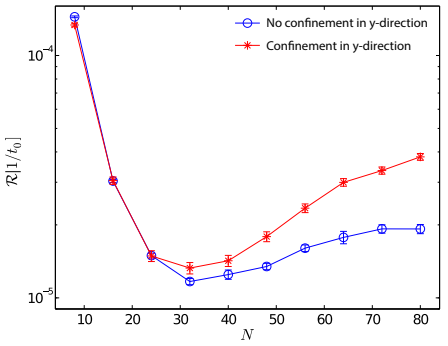

Figure 4.1. The escape rate of a self-avoiding polymer from the external potential of Eq. (2.22) without confinement in y-direction and from the confining external potential of Eq. (2.21). The decreasing escape rate shows a minimum at the chain length $N = 32$ after which it starts to increase. Increase in the escape rate for longer chains is more pronounced in the potential with y-directional confinement.

Figure 4.2 also shows the effective potentials at the barrier top. In the confining external potential, the effective potential at the barrier top is increasing while in the potential without the y-directional confinement it

starts to decrease after $N = 32$ indicating that the chain is more elongated at the barrier top. The same 'crowding' effect explains this: while the centre of the mass is still at the barrier top, most of the chain is still in the initial well and cannot 'fit' in the well same way as it can fit into the external potential without the confinement in the y-direction, where it has more space to spread out. This 'crowding' effect is seen for self-avoiding chains only.

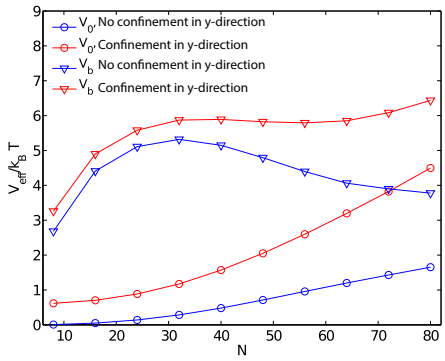

Figure 4.2. The effective external potentials at the minimum (circles) and at the barrier top (triangles), thermally averaged according to Eq. (3.22) in the both external potentials, with and without the y-directional confinement.

4.1.2 Escape rate in a confining potential

The escape rate of the polymer system was computed in the confining external potential of Eq. (2.21). The escape rate calculated from Kramers' Eq. (3.24), using both $E_{\text{eff}}(x_{\text{C}}, N)$ and $V_{\text{eff}}(x_{\text{C}}, N)$, is compared with the PIHD simulation rate in Fig. 4.3. Here, the rates obtained by the PIHD simulations present the correct results for the escape rate within the numerical errors.

Solving the escape rate with Kramers' Eq. (3.24) using both $E_{\text{eff}}(x_{\text{C}}, N)$ and $V_{\text{eff}}(x_{\text{C}}, N)$ results in the same escape rate for the ideal FENE chain. The escape rate of the ideal FENE chain decreases monotonically and Kramers' equation gives good agreement with PIHD simulations for chains of length $N < 24$. Kramers' equation overestimates the rate for ideal chains longer than this, yet still producing qualitatively correct rates.

The escape rates obtained with Kramers' Eq. (3.24) for the self-avoiding FENE chain differ more from the PIHD simulation rates. Kramers' Eq. (3.24) clearly overestimates rates for chains longer than $N = 32$. The difference in the escape rate with PIHD simulations is larger when the escape rate is obtained using $E_{\text{eff}}(x_{\text{C}}, N)$. This indicates that the reaction

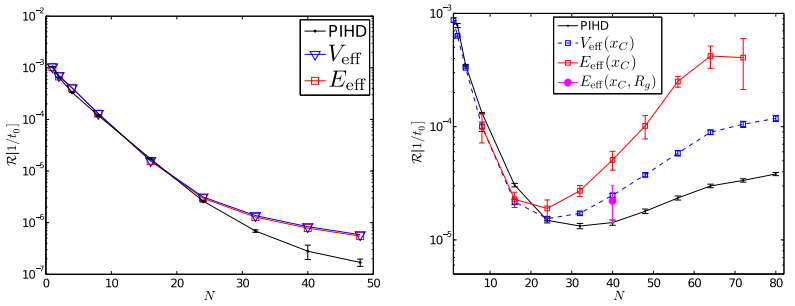

Figure 4.3. The polymer escape rate from the confining two-dimensional external potential of Eq. (2.21) for the ideal FENE chain model (left panel) and for the self-avoiding FENE chain model (right panel). The ideal chain model shows monotonic decrease and fairly good agreement between the PIHD simulation and Kramers' rate for the short chains. For the self-avoiding chain model, the curve obtained using the effective potential energies and Kramers' Eq. (3.24) is qualitatively similar to curve obtained by PIHD but vastly overestimates the rate for the longer chains. The purple dot represents the rate estimate obtained by averaging the potential energy over a tilted line shown in Fig. 4.5.

coordinate for the escape process is not defined accurately enough.

The curves for the effective potentials $E_{\mathrm{eff}}(x_{\mathrm{C}}, N)$ and $V_{\mathrm{eff}}(x_{\mathrm{C}}, N)$ are thermally averaged according to Eq. (3.22) and are shown in Fig. 4.4. The parameters $\omega_{0,\mathrm{eff}}(N)$, $\omega_{B,\mathrm{eff}}(N)$ and $\Delta E_{\mathrm{eff}}(N)$ for Eq. (3.24) were obtained by fitting parabolas, shown in red and green, to the minima and maxima of the curves.

Figure 4.5 shows the total potential energy surface $E_{\mathrm{eff}}(x_{\mathrm{C}}, R_g, N)$ as a function of the x-coordinate of the centre of mass x_{C} and the radius of gyration R_g, sampled according to Eq. (3.25) for self-avoiding FENE chains of length $N = 8$ and $N = 40$. In the figure it can be seen that the energy barrier of the escape for the polymer of length $N = 8$ follows a vertical line and therefore the escape event is likely to happen in a coiled state; the radius of gyration of the polymer does not increase when moving to the barrier top. For the chain of length $N = 40$ the figure shows that the energy barrier is tilted and the polymer tends to stretch out at the top of the barrier. The minimum energy path of the escape is trough the region of a larger radius of gyration. Tilting of the energy barrier is the reason why the one-dimensional reaction coordinate is not sufficient to describe the actual escape event. The curves of Fig. 4.4 do not include the effect of the tilted energy barrier and the activation energy is too low leading to an overestimate of the escape rate as shown in Fig. 4.3 (right panel). The escape rate estimate is improved when the energy at the barrier top is

averaged over the tilted line in Fig. 4.5 (right panel). This is shown with the purple dot in Fig. 4.3 (right panel).

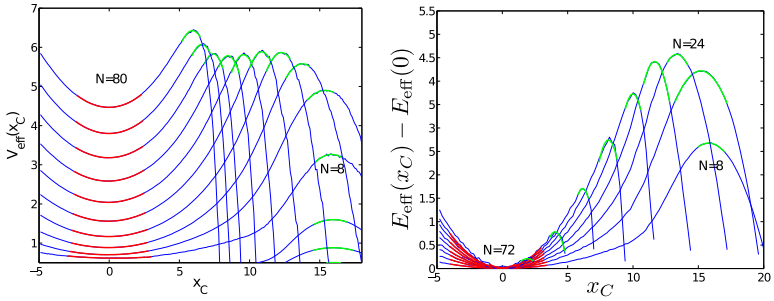

Figure 4.4. The effective external potential $V_{\rm eff}(x_{\rm C}, N)$ (left panel) and effective total energy $E_{\rm eff}(x_{\rm C}, N)$ (right panel) curves for chain lengths $N = 8, \ldots, 80$. $E_{\rm eff}(0, N)$ increases linearly with N, approximately as $E_{\rm eff}(0, N) \approx 9N$, so the effective energy at the minimum $E_{\rm eff}(0, N)$ is reduced from each curve to fit the curves in the same figure. The red and green lines represent parabolic fits to the minima and maxima which are used to calculate $\omega_{0,\rm eff}(N)$, $\omega_{B,\rm eff}(N)$, and $\Delta E_{\rm eff}(N)$ for Eq. (3.24).

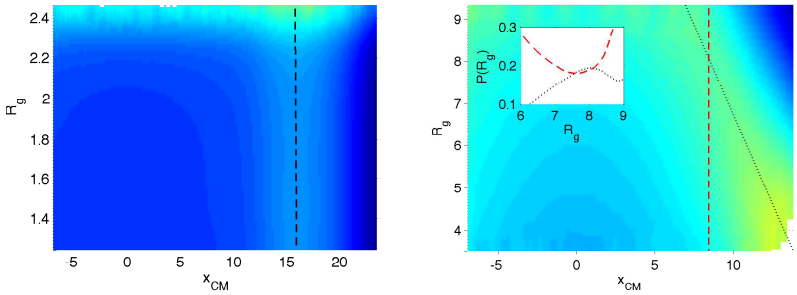

Figure 4.5. The effective energy landscape $E_{\rm eff}(x_{\rm C}, R_g, N)$ according to Eq. (3.25) as a function of the centre of mass and the radius of gyration of a polymer of length $N = 8$ (left panel) and $N = 40$ (right panel). The dashed lines represent the case when the reaction coordinate is defined using the centre of mass only. For the chain of length $N = 8$ the energy barrier closely follows the dashed line and a good reaction coordinate can be defined using the centre of mass only. For the polymer of length $N = 40$ the energy barrier is tilted, and the centre of mass based reaction coordinate leads to undersampling of the saddle point region and underestimates the activation energy. A two-dimensional reaction coordinate can be defined and averaging at the barrier can be done along the dotted line giving a higher activation energy. Thermal averaging along the dotted line samples the saddle point region correctly as it is shown in the inset where the probabilities along the lines are plotted. The purple dot in Fig. 4.3 presents the rate computed by averaging over the tilted dotted line.

4.2 Escape in a double well potential

In Publication II and Publication III the escape of an ideal harmonic polymer from a one-dimensional potential well was studied. The escape rate was computed using Brownian dynamics (BD) simulations of Eq. (2.4), Langevin dynamics (LD) simulations of Eq. (2.2), forward flux sampling (FFS) of Eq. (3.19), and the harmonic transition state theory (HTST) of Eq. (2.25) accompanied with dynamical corrections (DC). The DC were computed using the methodology by Voter and Doll [29], and a novel method based on FFS described in Sec. 3.4.1. The external potential well was given by Eq. (2.20) and was the same as used by Lee and Sung [15].

The BBK integration scheme of Eq. (3.3) was used for LD with a time step of $\delta t = 0.005$ and the forward Euler integration of Eq. (3.4) for BD with a time step $\delta t = 0.01$. Chains with different number of beads N in the range $N \in \{1, \ldots, 120\}$ were simulated with parameters $\gamma = 1.0$, $m = 1.0$ and $k_B T = 1.0$. The parameters for the external potential of Eq. (2.20) were $\omega^2 = 1.5$ and $a_0^2 = 1.5$. The parameters are the same as those used in Ref. 15. If we choose the units of length, mass and energy to be $l_0 = 1.02$ nm, $m_0 = 1870$ amu, corresponding to a double stranded DNA, and $k_B T$ at $T = 300$ K, the unit of time becomes $t_0 = \sqrt{m_0 l_0^2 / k_B T} = 27.9$ ps. The LD and BD simulations were performed sampling 1 000 - 240 000 trajectories depending on the chain length.

4.2.1 Minimum energy paths and saddle points

To obtain the escape rate using HTST the initial minimum and the saddle points of the escape transition needs to be known. The minimum energy path (MEP) containing the initial minimum and the saddle point of escape was computed using the Nudged Elastic Band (NEB) method. The MEPs for chains of length $N = \{1, 16, 64, 120\}$ as a function of the centre of mass X_0 for the chains with spring constants $K = 10$ and $K = 60$ are shown in the left panel of Fig. 4.6. The barrier height as a function the chain length N for the chains with spring constant $K = 10$ and $K = 60$ is shown in the right panel of Fig. 4.6.

The height of the energy barrier increases linearly with N until it reaches a critical value $\tilde{N}_C$, where tilde denotes an integer value. The critical value N_C is solved for the continuum chain model in the same external potential and the value of N_C is given by Eq. (2.27). Computed with MEP, the critical value is $\tilde{N}_C = 8$ for the chain with $K = 10$, and $\tilde{N}_C = 20$ for

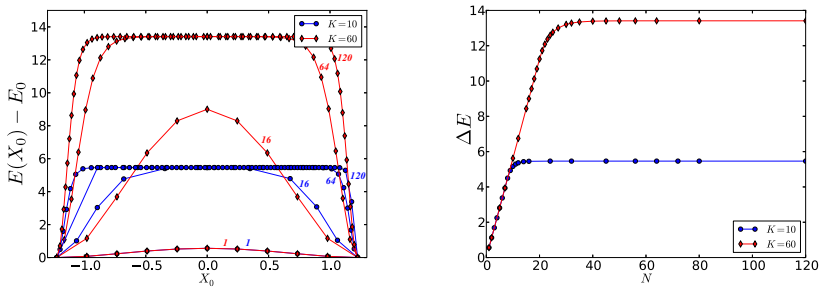

Figure 4.6. Left panel: The minimum energy paths (MEP) visualised as a function of the centre of mass X_0 for ideal chains of length $N = \{1, 16, 64, 120\}$ and harmonic spring constants $K = 10$ and $K = 60$. Right panel: The barrier height along the MEP as a function of the chain length N. The energy barrier increases linearly with increasing N until it reaches $\tilde{N}_C$ after which it saturates. After this, the barrier starts to flatten out and the activation energy does not increase any more.

the chain with $K = 60$. This is in good agreement with the analytical expression of Eq. (2.27), which gives $N_C = 8.11$ for $K = 10$ and $N_C = 19.86$ for $K = 60$.

For chains of length $N < \tilde{N}_C$ the saddle point corresponds to a configuration where the polymer lies in a coiled state on top of the barrier: all beads are on top of each other. For the longer chains, $N > \tilde{N}_C$, the polymer stretches out and energy barrier quickly saturates to a plateau. In this region, the negative eigenvalue $\lambda_1^\ddagger$ of the unstable mode approaches zero as the barrier along this mode flattens out. This is shown in the left panel of Fig. 4.7. The smallest positive eigenvalue $\lambda_2^\ddagger$, whose eigenmode is responsible of the stretching of the chain, decreases until $\tilde{N}_C$ after which it starts to increase. With increasing $N > \tilde{N}_C$ the eigenvalue $\lambda_2^\ddagger$ saturates to a constant value.

The right panel of Fig. 4.7 illustrates the eigenmodes $\mathbf{s}_1$ and $\mathbf{s}_2$ (eigenvectors of the Hessian $\mathbf{H}_\ddagger$) at the saddle point for a chain of length $N = 56$. The red triangular arrows illustrate the movement of the chain towards the final state along the eigenmode $\mathbf{s}_1$. The blue square arrows show that the eigenmode $\mathbf{s}_2$ causes stretching of the chain.

4.2.2 Dynamical rate and harmonic transition state theory

The escape rate of an ideal harmonic polymer chain from the external potential of Eq. (2.20) was computed with LD and BD simulations, using equations of motion (2.3) and (2.4), respectively. The criterion for the escape event was that the centre of mass of the polymer has reached

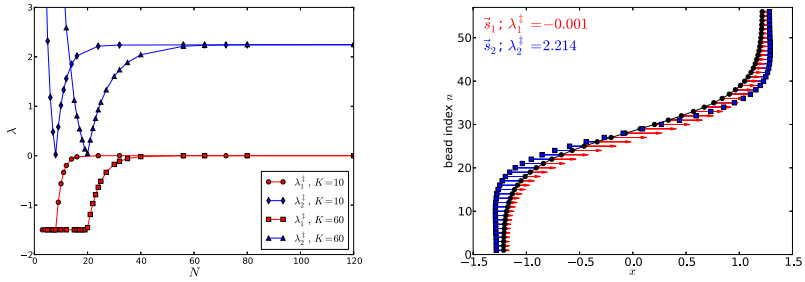

Figure 4.7. Left panel: The two lowest eigenvalues of the Hessian matrix $\mathbf{H}_\ddagger$ at the saddle point for chains with harmonic spring constants $K = 10$ and $K = 60$. The negative eigenvalue $\lambda_1^\ddagger$ corresponding to the unstable mode approaches zero after $\tilde{N}_C$. The smallest positive eigenvalue $\lambda_2^\ddagger$ decreases until $\tilde{N}_C$ after which it starts increasing and saturates to a constant value. The eigenmode corresponding to $\lambda_2^\ddagger$ is responsible for the chain stretching after $\tilde{N}_C$. Right panel: Visualisation of the two lowest eigenmodes at the saddle point for a chain of length $N = 56$ and spring constant of $K = 60$. The location of the beads at the saddle point are marked with black dots and the eigenvector $\mathbf{s}_1$ is marked with red triangular arrows and eigenvector $\mathbf{s}_2$ with blue square arrows.

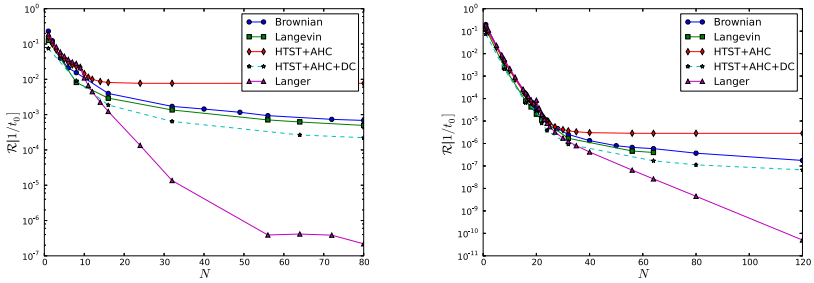

Figure 4.8. The escape rate $\mathcal{R}$ obtained from BD simulations (circles), LD simulations (squares), HTST with AHC (diamonds) accompanied with dynamical corrections (stars) computed according to Voter and Doll [29], and Langer's rate theory (triangles). The chain with spring constant $K = 10$ is shown on the left panel and the chain with spring constant $K = 60$ is shown on the right panel. Langer's theory underestimates the escape rate in the region $N > \tilde{N}_C$ where the unstable mode $\lambda_1^\ddagger$ appearing in the prefactor of Eq. (2.35) approaches zero as the barrier flattens out. For chains $N \geq 56$ with spring constant $K = 10$ there is numerical inaccuracy in Langer's rate, because the unstable mode $\lambda_1^\ddagger < 10^{-9}$ is close to zero.

$X_0 = a_0/2$. Using this criterion the escape probability curve was computed according to Eq. (3.1). The actual escape rate was computed using Eq. (3.2). An example of the $P_{\mathrm{esc}}(t)$ curve of Eq. (3.1) and a linear fit to it is shown in Fig. 3.1. In the figure, the curve is for a self-avoiding chain, but it is similar for an ideal chain as well.

The escape rate obtained by MD simulations, using both BD and LD, is compared with the escape rate by HTST with DC in Fig. 4.8. The HTST

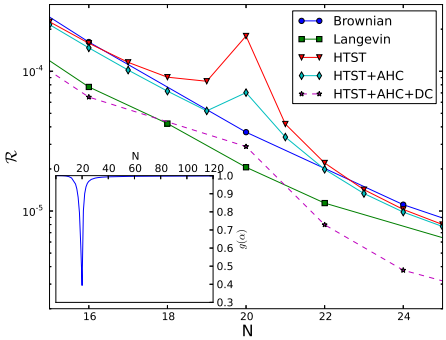

Figure 4.9. The escape rate calculated for polymers with spring constant of $K = 60$ as a function of the chain length N close to the crossover, $\tilde{N}_C$. Circles and squares indicate results obtained from MD simulations using Brownian and Langevin dynamics, respectively. Triangles indicate HTST rate estimates (Eq. (2.25)), diamonds estimates from HTST with anharmonic corrections (Eq. (2.29)), and stars estimates HTST with AHC and DC (Eq. (2.31)). The anharmonic correction factor $g(\alpha)$, shown in the inset, is given by Eq. (2.28) and it significantly reduces the diverging peak in the HTST rate estimate.

is corrected with anharmonic corrections (AHC), according to Eq. (2.29), which reduces the divergence due to the smallest positive eigenvalue approaching zero at $\tilde{N}_C$. The effect of the AHC is shown in Fig. 4.9, where the divergence at $\tilde{N}_C$ in the HTST rate of Eq. (2.25) is reduced by the AHC of Eq. (2.28). The factor $g(\alpha)$ of Eq. (2.28) is shown in the inset, where it has mostly the value of 1.0, but a sharp peak at N_C, which reduces the divergence in the HTST rate.

The escape rate from HTST of Eq. (2.29) reaches a plateau quickly after $\tilde{N}_C$. This is due to the energy barrier reaching its maximum height and the polymer at the saddle point taking a stretched configuration as illustrated in Figs. 4.6 and 4.7. In this region of a flat barrier, the influence of the DC becomes relevant. The DC here is computed according to method of Eq. (2.30) by Voter and Doll [29][1]. The dynamically corrected HTST rate reaches good agreement with the rate obtained from LD and BD simulations within a factor of two.

The escape rate given by the Kramers-Langer Eq. (2.35) significantly underestimates the escape rate in the region $N > \tilde{N}_C$ for chains with both spring constants, $K = 10$ and $K = 60$. In Langer's expression for the escape rate, there is a prefactor that includes $|\lambda_1^{\ddagger}|$. For the systems ex-

[1]Note that in this calculation, the correct Maxwellian-flux distribution for the perpendicular component of the velocity was not used. Instead, all the velocities were taken from the Maxwellian distribution. However we have computed the correct DC using a method based on FFS in Sec. 4.2.3.

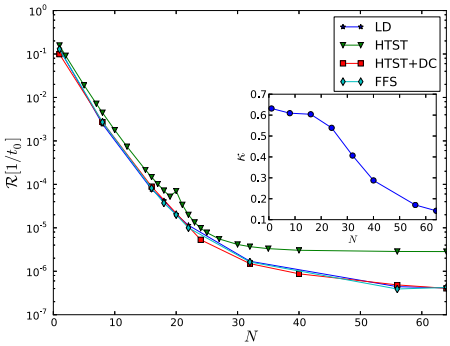

Figure 4.10. The escape rate obtained by LD (stars), by HTST (triangles) accompanied with DC using FFS (squares) and by solving the escape rate using only FFS (diamonds). The inset shows the dynamical correction factor κ. HTST with DC computed using FFS gives excellent agreement with LD simulations as does the rate computed by FFS only.

hibiting a flat barrier, the eigenvalue of the unstable mode $\lambda_1^\ddagger$ approaches zero resulting in a drastic underestimate of the escape rate.

4.2.3 Forward flux sampling

In Publication III, the escape rate of a harmonic ideal polymer in the external double potential well potential of Eq. (2.20) was also computed using the Forward Flux Sampling (FFS) methodology described in Sec. 3.4. The escape rate obtained by FFS agrees quantitatively with the rate obtained from Langevin dynamics simulations as shown in Fig. 4.10.

In addition, we calculated the dynamical correction factor κ for HTST using the FFS methodology described Sec. 3.4.1. Using the FFS method the DC factor κ is given by Eg. (3.21). The dynamically corrected HTST rate agrees quantitatively with the LD simulations.

4.2.4 Efficiency analysis

In Publication III, the computational efficiency of solving the escape rate of a harmonic ideal polymer chain in the external double well potential was examined with four methods: molecular dynamics simulations using LD, FFS, and HTST with DC, where the DC were computed using methodology by Voter and Doll [29] (VDDC) and FFS type algorithm of Sec. 3.4.1 (FFDC). To benchmark the computational efficiency, the number of force function evaluations used in each method was counted. Then we compared the number of function evaluations used in each method to

Method	$\Delta\mathcal{R}/\mathcal{R}$	# func. eval.
$N = 8$		
Direct LD	6 %	6.4×10^9
FFS (10 planes)	6 %	5.0×10^8
HTST+VDDC	3 %	8.0×10^7
HTST+FFDC	4 %	8.0×10^6
$N = 64$		
Direct LD	10 %	3.0×10^{13}
FFS (10 planes)	17 %	9.0×10^{11}
FFS (16 planes)	10 %	7.0×10^{11}
HTST+VDDC	9 %	2.6×10^{11}
HTST+FFDC	3 %	2.88×10^{10}

Table 4.1. Relative errors $\Delta\mathcal{R}/\mathcal{R}$ of the escape rate and the number of the force evaluations required for each method for polymers of length $N = 8$ and $N = 64$ at a temperature of T=1.0. The HTST+FFDC converges to an small relative error with the least computational effort, about an order of magnitude less than HTST+VDDC which in turn is about an order of magnitude more efficient than FFS. At this relatively high temperature, the direct Langevin dynamics simulation can be carried out to obtain an estimate of the escape rate and it turns out to be one to two orders of magnitude less efficient than FFS, depending on the length of the polymer.

reach the same level of statistical accuracy. The computational cost for ideal polymers of length $N = 8$ and $N = 64$ was evaluated. The statistical error was computed by repeating calculation several times and then using the standard deviation divided by $\sqrt{N_s}$ as an error estimate (standard error of the mean), where $\sqrt{N_s}$ is the number of independent samples. The results for $N = 8$ and $N = 64$ are shown in Table 4.1 at a temperature $T = 1.0$. For FFS with the chains of length $N = 8$ and $N = 64$ (16 planes), the sample size was $N_s = 20$ with each sample having 10 000 trajectories fired from each plane. For DC calculations $N_s = 10$ with 1000 trajectories fired from each plane.

For both chain lengths studied at the temperature of $T = 1.0$, FFS is an order of magnitude faster than direct LD simulations for obtaining the same level of statistical error, and HTST+VDDC is two orders of magnitude faster than direct LD simulations. HTST+FFDC is two orders of magnitude faster than direct LD simulations for $N = 64$ and three orders of magnitude faster for $N = 8$.

At the lower temperature of $T = 0.5$, direct LD simulations become impossible. In Table 4.2, the efficiency of FFS is compared with HTST+FFDC

Method	$\Delta\mathcal{R}/\mathcal{R}$	# func. eval.
FFS (20 planes)	20 %	9.3×10^{11}
HTST+FFDC	3 %	6.0×10^{10}

Table 4.2. Comparison of computational efficiency of FFS and HTST+FFDC at $T = 0.5$ for polymers with $N = 64$. Even with addition of extra hyperplanes in the small flux region, most of the FFS simulations fail in that at some point none of the trajectories make it to the next plane. The number of force evaluations reported here includes only the successful FFS calculations, so it present a lower bound for the number of function evaluations needed for the this level of accuracy.

for polymers of length $N = 64$. HTST+FFDC is an order of magnitude faster than FFS. At this temperature, most of the FFS simulation runs fail in that at some point none of the trajectories make it to the next plane. We optimised the FFS algorithm by adding extra planes to the region where the forward flux is small. This reduced the number of failed FFS simulation runs, but still most of the runs failed. The error estimate is obtained using only successful FFS simulation runs, so the number of force function evaluations represent the lower bound for required function evaluations.

According to Refs. 43 and 44 the FFS method can be optimised by adjusting the plane positions and by adjusting the number trial runs shot from each plane. For the chain of length $N = 64$ we optimised the plane positions so that six additional planes were positioned in the region where the forward flux $P(\lambda_{i+1}|\lambda_i)$ is small. In this region the potential gradient uphill is steep (see Fig. 4.6 left) and the majority of the trial runs fail to reach the next plane when the distance between the planes is large. With the optimisation procedure a smaller statistical error was obtained with a smaller number of time steps as is shown in Table 4.1.

The computational cost of HTST+FFDC comprises the cost of finding the MEP using the NEB method, the equilibration of initial configurations within the transition state hyperplane, and computing the forward flux for DC. MEP calculations typically took a few thousand time steps for the polymers, which is negligible here. In the computation of DC, 90 % of the computational cost comes from equilibrating the polymer within the transition state hyperplane, and the rest 10 % is the cost of computing the forward flux $P(\lambda_n|\lambda_0)$. It is possible that the time needed for equilibration could be reduced using more efficient algorithms such as stochastic collisions [45].

5. Summary and conclusions

The thesis has focused on the canonical polymer escape problem of various polymer models in two different external potentials. The first system is a two-dimensional asymmetric potential well with no minimum in the final state. In this system we have examined ideal and self-avoiding FENE-LJ polymers. The second system is a one-dimensional bistable external double well potential, where the harmonic ideal chain has been studied. We have examined the dynamics of the escape event, mainly the escape rate, but also the configurations which polymers take during escape have been studied.

In Publication I the seminal Kramers' escape problem for one particle was extended for polymers escaping from a two-dimensional external potential. Similar system has been previously studied by Shin *et al.* [18, 19]. We computed the escape rate using Path Integral Hyperdynamics (PIHD) simulations. With a proper choice of the bias potential PIHD produces numerically exact results with Langevin dynamics (LD). We compared the PIHD results for the escape rate with the Kramers' rate. Kramers' rate was obtained by using one-dimensional effective potentials as a function of the x-coordinate of the centre of mass, for both the total potential energy $E_{\text{eff}}(x_c)$ and the external potential energy $V_{\text{eff}}(x_c)$. Kramers' rate obtained by using the both effective potentials, $E_{\text{eff}}(x_c)$ and $V_{\text{eff}}(x_c)$, produces qualitatively correct behaviour of the escape rate as a function of the chain length N but overestimates the rate for longer polymers.

Kramers' estimate for the escape rate is better when the polymer chain is short, so that the polymer is in a coiled state during the escape process. Longer polymers tend to stretch out at the barrier top during the escape process. We sampled the two-dimensional effective energy landscapes of the polymer escape as a function of the x-coordinate of the centre of mass and the radius of gyration R_g, for the total potential energy $E_{\text{eff}}(x_c, R_g)$.

The two-dimensional energy surfaces show that the energy barrier for the escape is tilted for the longer polymers as shown in Fig. 4.5. Averaging the total energy at the barrier top over the tilted energy barrier improves the rate estimate as shown in Fig. 4.3. This indicates that a one-dimensional reaction coordinate is not sufficient to describe the dynamics of the polymer escape.

In Publication II a one-dimensional harmonic ideal polymer escaping from a one-dimensional bistable external double well potential was studied. The escape rate was computed by molecular dynamics simulations using Langevin dynamics (LD) and Brownian dynamics (BD). The escape rate was also calculated using the harmonic transition state theory [31] (HTST) with dynamical corrections (DC) obtained by the method proposed by Voter and Doll [29]. The escape rate results from HTST with DC were compared with MD. HTST with DC produces quantitative agreement in escape rate with the MD simulations within a factor of two.

In order to obtain the escape rate with HTST, the minimum energy path (MEP) of escape was determined for different chain lengths N using the Nudged Elastic Band method. We studied the eigenmodes of the Hessian matrices at the saddle point of the MEP to illustrate the dynamics of escape. The two lowest eigenmodes at the saddle point describe the dominant dynamics.

The lowest mode with a negative eigenvalue corresponds to the polymer moving towards the final state. This eigenvalue approaches zero when the chain length N increases. With this the energy barrier along the MEP flattens out, which makes Langer's estimate [9, 15] for the escape rate poor, since Langer's expression for the escape rate includes the negative mode as a prefactor describing recrossings back to the initial state.

The mode with the second lowest eigenvalue is responsible for the polymer stretching out at the saddle point after the critical length N_C. With increasing N, the eigenvalue of the second lowest mode decreases until N_C after which it starts to increase, saturating to a constant value. At the critical length N_C, the polymer starts to stretch out and the saddle point bifurcates into two saddle points. This is analogous to the appearance of an instanton solution in quantum mechanical rate theories based on the Feynman path integral describing tunnelling process of a particle. At the critical length N_C, the second lowest eigenvalue approaches zero causing the divergence in the escape rate. This divergence was mostly eliminated by introducing anharmonic corrections [15].

In Publication III, we solved the escape rate using forward flux sampling (FFS) and HTST with DC. With these two methods we obtained quantitative agreement in the escape rate with LD simulations. DC were computed with a novel method based on FFS, where the DC factor κ is computed by sampling the dynamics between the planes, placed between the transition state hyperplane and a hyperplane in the final state. We compared numerical efficiency of the three methods: LD, FFS, HTST with DC. To obtain the same level of statistical error, we found that FFS is an order of magnitude faster than LD and HTST with DC two orders of magnitude faster than LD.

For the work presented here, one possible future direction is a full transition state theory (TST) calculation of the rate in the systems studied here. Another interesting prospect is to extend the problem to more realistic three-dimensional systems. Performing full hydrodynamic calculation using for example the fluctuating lattice-Boltzmann method [22] would also make the system more realistic.

References

[1] V. V. Palyulin, T. Ala-Nissila, and R. Metzler, *Soft Matter*, **10**, 9016 (2014).

[2] M. Muthukumar, *'Polymer Translocation'*, Taylor & Francis; Boca Raton U.S.A. (2011).

[3] J. J. Kasianowicz, E. Brandin, D. Branton, and D.W. Deamer, *Proc. Natl. Acad. Sci. U.S.A.* **93**, 13770 (1996).

[4] J. Han, S. Turner and H. Craighead *Phys. Rev. E* **83**, 1688 (1999).

[5] X. Liu, M. M. Skanata, D. Stein, *Nat. Commun.* **6**, 6222 (2014).

[6] S. Howorka, S. Cheley, and H. Bayley, *Nature Biotechnology* **19**, 636 (2001).

[7] M. B. Mikkelsen, W. Reisner, H. Flyvbjerg, and A. Kristensen, *Nano Lett.* **11**, 1598 (2011).

[8] H. A. Kramers, *Physica* **7**, 284 (1940).

[9] J. S. Langer, *Ann. Phys. (N.Y.)*, **54**, 258 (1969).

[10] P. J. Park, and W. Sung *J. Chem. Phys.* **111**, 5259 (1999).

[11] K. L. Sebastian, *Phys. Rev. E* **61**, 3245 (2000).

[12] K. L. Sebastian and A. K. R. Paul, *Phys. Rev. E* **62**, 927 (2000).

[13] K. L. Sebastian and A. Debnath, *J. Phys.: Cond. Matt.* **18**, S283 (2006).

[14] A. Debnath, A. K. R. Paul and K. L. Sebastian, *J. Stat. Mech.* **11**, S11024 (2010).

[15] S. K. Lee and W. Sung, *Phys. Rev. E* **63**, 021115 (2001).

[16] S. K. Lee and W. Sung, *Phys. Rev. E* **64**, 041801 (2001).

[17] A. K. R. Paul, *Phys. Rev. E* **72**, 061801 (2005).

[18] J. Shin, T. Ikonen, M. D. Khandkar, T. Ala-Nissila, and W. Sung, *J. Chem. Phys.* **133**, 184902 (2010).

[19] T. Ikonen, Dynamics of Escape and Translocation of Biopolymers, PhD thesis, Aalto University, School of Science, (2012).

[20] G. S. Grest, K. Kremer, *Phys. Rev. A* **33** 3628(R) (1986)

[21] K. Kremer, G. S. Grest, *J. Chem. Phys.* **92** 5057 (1990)

[22] S. T. Ollila, C. Denniston, M. Karttunen, T. Ala-Nissila, *J. Chem. Phys.*, **134(6)**, 064902-064902 (2011)

[23] M. Doi, S. F. Edwards, *'The theory of polymer dynamics'*, Clarendon Press; Oxford U.S.A. (1986).

[24] A. Kopf, B. Dünweg and W. Paul *J. Chem. Phys.* **107** 6945 (1997).

[25] H. Pelzer, and E. Wigner, *Z. Phys. Chem. B* **15**, 445 (1932)

[26] E. Wigner, *Trans. Faraday Soc.* **34**, 29 (1938).

[27] J.C. Keck., *J. Chem. Phys.* **32**, 1035 (1960).

[28] J.C. Keck., *Farad. Discuss.* **33**, 173 (1962).

[29] A. F. Voter and J. D. Doll, *J. Chem. Phys.* **82**, 80 (1985).

[30] C. Wert and C. Zener, *Phys. Rev.* **76**, 1169 (1949)

[31] G. H. Vineyard, *J. Phys. Chem. Solids* **3**, 121 (1957).

[32] P. Hänggi, P. Talkner, and M. Borkovec, *Rev. Mod. Phys.* **62**, 251 (1990).

[33] A. Brünger, C. Brooks, M. Karplus, *Chem. Phys. Lett.* **105**, 495 (1984).

[34] J. Izaguirre, D. Catarello, J. Wozniak, *J. Chem. Phys.* **114** 2090 (2001).

[35] L. Y. Chen and N. J. M. Horing, *J. Chem. Phys.* **126**, 224103 (2007).

[36] T. Ikonen, M. Khandkar, L. Chen, S. Ying, and T. Ala-Nissila, *Phys. Rev. E* **84**, 026703 (2011).

[37] G. Henkelman and H. Jónsson, *J. Chem. Phys.* **113**, 9978 (2000).

[38] G. Henkelman, B. Uberuaga and H. Jónsson, *J. Chem. Phys.* **113**, 9901 (2000).

[39] H. Jónsson, G. Mills, and K. W. Jacobsen. Nudged elastic band method for finding minimum energy paths of transitions, In Classical and Quantum Dynamics in Condensed Matter Simulations; Berne, B.J.; Ciccotti, G.; Coker, D.F., Eds.; World Scientific: Singapore, 1998; pp 397.

[40] R. J. Allen, P. B. Warren, and P. R. ten Wolde, *Phys. Rev. Lett.* **94**, 018104 (2005).

[41] R. J. Allen, D. Frenkel, and P. R. ten Wolde, *J Chem. Phys.* **124**, 024102 (2006).

[42] R. J. Allen, D. Frenkel, and P. R. ten Wolde, *J. Chem. Phys.* **124**, 194111 (2006).

[43] R. J. Allen, C. Valeriani, P. R. ten Wolde, *J. Phys.: Condens. Matter* **21**, 463102 (2009).

[44] E. E. Borrero, F. A. Escobedo, *J. Chem. Phys.* **129**, 024115 (2008).

[45] H. C. Andersen, *J. Chem. Phys.* **72**, 2384 (1980).

Aalto-DD 143/2016

ISBN 978-952-60-6925-8 (printed)
ISBN 978-952-60-6924-1 (pdf)
ISSN-L 1799-4934
ISSN 1799-4934 (printed)
ISSN 1799-4942 (pdf)

Aalto University
School of Science
Department of Applied Physics
www.aalto.fi

BUSINESS +
ECONOMY

ART +
DESIGN +
ARCHITECTURE

SCIENCE +
TECHNOLOGY

CROSSOVER

DOCTORAL
DISSERTATIONS